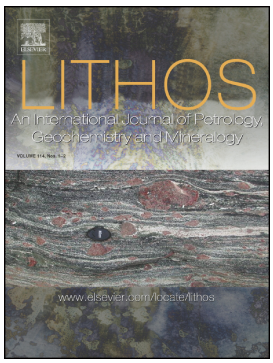

Early Cretaceous high-Ti and low-Ti mafic magmatism in Southeastern Tibet: Insights into magmatic evolution of the Comei Large Igneous Province

Yaying Wang, Lingsen Zeng, Paul Asimow, Li-E Gao, Chi Ma, Paula Antoshechkina, Chunli Guo, Kejun Hou, Suohan Tang

PII: S0024-4937(17)30397-3
DOI: doi:10.1016/j.lithos.2017.11.014
Reference: LITHOS 4475

To appear in:

Received date: 5 May 2017
Accepted date: 12 November 2017

Please cite this article as: Yaying Wang, Lingsen Zeng, Paul Asimow, Li-E Gao, Chi Ma, Paula Antoshechkina, Chunli Guo, Kejun Hou, Suohan Tang , Early Cretaceous high-Ti and low-Ti mafic magmatism in Southeastern Tibet: Insights into magmatic evolution of the Comei Large Igneous Province. The address for the corresponding author was captured as affiliation for all authors. Please check if appropriate. Lithos(2017), doi:10.1016/j.lithos.2017.11.014

Early Cretaceous high-Ti and low-Ti mafic magmatism in Southeastern Tibet: Insights into magmatic evolution of the Comei Large Igneous Province

Yaying Wang[1], Lingsen Zeng[1], Paul Asimow[2], Li-E Gao[1], Chi Ma[2], Paula Antoshechkina[2], Chunli Guo[3], Kejun Hou[3], Suohan Tang[1]

1. Institute of Geology, Chinese Academy of Geological Sciences, Beijing 100037, China

2. Division of Geological and Planetary Sciences, California Institute of Technology, Pasadena, California 91125, USA

3. Institute of Mineral Resources, Chinese Academy of Geological Sciences, Beijing 100037, China

ABSTRACT: The Dala diabase intrusion, at the southeastern margin of the Yardoi gneiss dome, is located within the outcrop area of the ~132 Ma Comei Large Igneous Province (LIP), the result of initial activity of the Kerguelen plume. We present new zircon U-Pb geochronology results to show that the Dala diabase was emplaced at ~132 Ma and geochemical data (whole-rock element and Sr-Nd isotope ratios, zircon Hf isotopes and Fe-Ti oxide mineral chemistry) to confirm that the Dala diabase intrusion is part of the Comei LIP. The Dala diabase can be divided into a high-Mg/low-Ti series and a low-Mg/high-Ti series. The high-Mg/low-Ti series represents more primitive mafic magma compositions that we demonstrate are

parental to the low-Mg/high-Ti series. Fractionation of olivine and clinopyroxene, followed by plagioclase within the low-Mg series, lead to systematic changes in concentrations of mantle compatible elements (Cr, Co, Ni, and V), REEs, HFSEs, and major elements such as Ti and P. Some Dala samples from the low-Mg/high-Ti series contain large ilmenite clusters and show extreme enrichment of Ti with elevated Ti/Y ratios, likely due to settling and accumulation of ilmenite during the magma chamber evolution. However, most samples from throughout the Comei LIP follow the Ti-evolution trend of the typical liquid line of descent (LLD) of primary OIB compositions, showing strong evidence of control of Ti contents by differentiation processes. In many other localities, however, primitive magmas are absent and observed Ti contents of evolved magmas cannot be quantitatively related to source processes. Careful examination of the petrogenetic relationship between co-existing low-Ti and high-Ti mafic rocks is essential to using observed rock chemistry to infer source composition, location, and degree of melting.

Keywords: Comei Large Igneous Province, Mafic magmatic evolution, LLD, Low-Ti and high-Ti mafic rocks, Tethyan Himalaya

1. INTRODUCTION

Many Large Igneous Provinces (LIPs) including the Karoo, Paraná-Etendeka, Siberian Traps and Emeishan consist of high-Ti (TiO_2 > 2.5 wt%) and low-Ti (TiO_2 < 2.5 wt%) series of mafic rocks with approximately similar ages but different distributions (Cox et a., 1967 & 1988; Lightfoot et al., 1993; Gibson et al., 1995 &

1996; Peate 1992; Peate and Hawkesworth, 1996; Xu et al., 2001 & 2004; Xiao et al., 2004; Ewart et al., 2004; Ren et al., 2017). These characteristics have led to vastly different petrogenetic models that attempt to explain the relationship between the high-Ti and low-Ti series, which can be summarized as: (1) different source regions, including complex interactions between plume, lithosphere, and asthenosphere (Walker et al., 1990; Hergt et al., 1991; Lightfoot et al., 1993; Gibson et al., 1995 & 1996); (2) different degrees of partial melting of a mantle plume source (Fodor et al., 1987; Xu et al., 2001 & 2004; Lai et al., 2012; Ren et al., 2017); (3) different degrees of crustal contamination (Shellnutt et al., 2011); or (4) the collective effects of all of the above factors (Petrini et al., 1987; Xiao et al., 2004; Ewart et al., 2004; Wang et al., 2007). In much of the cited work, TiO_2 content and Ti/Y ratio have been viewed as critical criteria for classifying mafic rocks and as indicators of their source characteristics (Cox et a., 1967 & 1988; Peate et al., 1992; Gibson et al., 1995 & 1996; Xu et al., 2001 & 2004).

However, during basaltic magma evolution, variations in liquid TiO_2 content can be a complex function of conditions (temperature, pressure, and oxygen fugacity) that influence the precipitation and fractionation of Fe-Ti oxide minerals (Hellman and Green, 1979; Ryerson and Watson, 1987; Snyder et al., 1993; Toplis et al., 1995 & 1996), as shown by many experimental results (Juster et al., 1989; Hess, 1993; Botcharnikov et al., 2008). Therefore, fractional crystallization processes rather than source composition or degree of partial melting may be the primary influence on Ti contents in LIP basalts. This idea has already been addressed in the well-studied

Emeishan LIP (Xu et al., 2003; Hao et al., 2004; Hou et al., 2011). Xu et al. (2003) and Hao et al (2004) proposed that primitive Emeishan magmas experienced, in some localities, early Fe-Ti oxide fractionation leading to a calc-alkaline or Bowen fractionation trend to form the low-Ti evolved basalts, whereas in other localities in the same province, the fractionation of Fe-Ti oxide phases was delayed, leading to a tholeiitic or Fenner differentiation trend and high-Ti evolved basalts. Xu et al. (2003) attributed the divergent evolution pathways to different oxidation states due to different degrees of assimilation of oxidized crustal components. Hou et al. (2011), however, revisited this issue, rejecting the idea of spatial and temporal organization of the two types within the Emeishan province in favor of a chemical distinction between coexisting high-Mg/low-Ti and low-Mg/high-Ti suites. In this case, informed by differentiation models, Hou et al. (2011) favored a co-genetic origin, with low-Mg/high-Ti basalts formed from high-Mg/low-Ti basalts by fractionation of olivine, pyroxene and plagioclase without Fe-Ti oxides. The Emeishan case shows, then, that the same data have been taken to support divergent models of the origin of TiO_2 and Ti/Y variations in mafic rocks. More case studies, supported by comprehensive chemical analyses of associated high-Ti and low-Ti rocks and quantitative fractionation models, are needed to investigate whether and when Ti contents can be used as robust indicators of magmatic sources or tectonic settings.

We consider this question using a well-characterized suite of mafic samples from the Tethyan Himalaya (Fig.1), part of the Himalaya orogenic belt. The Tethyan Himalaya is characterized by well-developed Paleozoic to Cenozoic sediments,

spectacular semi-continuous gneiss (or granitic) domes, and widespread mafic intrusions and dike swarms of various ages and geochemical characteristics. These rocks witnessed the breakup of the Gondwana supercontinent, seafloor spreading of the Tethyan Ocean, fore-arc hyperextension during the northward subduction of the Neo-Tethyan oceanic lithosphere, and the final continental collision between the Indian and the Eurasian Plate (Bhat, 1984; Vannay and Spring, 1993; Garzanti, 1993 & 1999; Williams et al., 2001; Chauvet et al., 2008; Zhu et al., 2008 & 2009; Zeng et al., 2012a & b, 2015a, 2017; Liu et al., 2013; Liu et al., 2015; Ji et al., 2016). They preserve critical records of deformation, magmatism, and metamorphism of the passive continental margin of eastern Gondwana.

Based on regional correlations of age and geochemical characteristics, Zhu et al (2009) proposed the existence of a large igneous province, the early Cretaceous Comei-Bunbury LIP, which includes mafic intrusions and dike swarms in the Comei-Cona-Yamdrok areas of the eastern Tethyan Himalaya as well as the Bunbury basalts in southwestern Australia (Fig. 1). These exposures may represent the eroded, deformed, and displaced remnants of a LIP associated with the breakup of the eastern Gondwana supercontinent upon impact of the initial phase of the Kerguelen mantle plume in Early Cretaceous time. However, many mafic rocks were included in this LIP without sufficient age or geochemical constraints to confirm the association. Some mafic rocks in the general area formed before ~190 Ma and others after ~80 Ma and clearly should not be included in the LIP (Zeng et al., 2012b). Available data also show that those mafic rocks that are associated with the Comei-Bunbury LIP include

both low-Ti (TiO_2 < 2.5 wt%) and high-Ti (TiO_2 > 2.5 wt%) series (Fig. 1, Zhu et al., 2007 & 2008; Xia et al., 2014; Liu et al., 2015; Wang et al., 2016). Determining whether these low-Ti and high-Ti mafic rocks are co-genetic or represent different magmatic suites requires careful geochronological and geochemical investigation.

In this contribution, we present new zircon U-Pb age and Hf isotope ratio data, whole-rock element concentration and isotope ratio (Sr and Nd) results as well as Fe-Ti oxide (ilmenite) electron probe (EPMA) data for high-Ti and low-Ti basaltic rocks from a relatively large diabase intrusion in the Dala area, Tethyan Himalaya, south Tibet (Figs. 1 & 2). We use these data to test (1) whether the low-Ti and high-Ti suites and the Comei and Yamdrok mafic rocks share a common age, (2) whether the low-Ti and high-Ti samples are isotopically similar, (3) whether the coexisting high-Ti and low-Ti rocks in Dala can be explained by a continuous fractionation evolution trend from one magma, and (4) whether the identified magmatic evolution path is common to other outcrops in the Comei LIP. The broader overall goal is to examine how TiO_2 varies in LIP-related mafic magmas during magmatic differentiation and to constrain what robust insights about source-level processes can be drawn from TiO_2 content of mafic magmas in general.

2. GEOLOGIC BACKGROUND AND SAMPLE DRESCRIPTIONS

The Dala diabase outcrops along the southeastern margin of the Yardoi gneiss dome in the eastern Tethyan Himalaya. The regional geology is similar to the margins of other Himalayan gneiss domes, featuring a thick sedimentary pile of early Triassic to late Cretaceous turbidites, fine-grained sandstones, shales, slates, and the Tethyan

Himalaya sequence (Liu and Ensele, 1994; Garzanti, 1999; Dai et al., 2008; Li et al., 2010; Cai et al., 2016). Since the onset of collision between the Indian and Eurasian plates, these sediments have undergone multiple phases of structural deformation, sub-greenschist facies metamorphism, and intrusion by magmas of basaltic to granitic composition (Aikman et al., 2008; Qi et al., 2008; Zeng et al., 2009, 2011a & b, 2012a, 2015b & 2016; Hou et al., 2012; Gao et al., 2009 & 2012; Xie et al., 2010; Webb et al., 2013; Diedesch et al., 2016). Around the Dala area, cross-cutting relationships show that there are at least four episodes of magmatism (Figs. 1 & 2). The earliest episode is represented by a late Permian pluton of diabase composition with a zircon U-Pb age of 273.0±2.2 Ma (Zeng et al., 2012b), intruding into the shale and sandstone formation. The diabase pluton of this study (Fig. 2) is from the second episode and intruded into the Triassic shale formation. This diabase, in turn, was later intruded by the third phase, early Eocene two-mica granites (Qi et al., 2008; Xie et al., 2010; Zeng et al., 2011a), and the fourth phase, granodioritic dykes of unknown age (Fig. 2).

To identify the formation age and characterize the geochemical nature of the Dala diabase, we collected samples along two transects across the pluton as shown in Fig. 2. Samples from both transects, except for the large contrast in grain sizes, consist of similar mineral assemblages including hornblende, plagioclase, and ilmenite with accessory phases of apatite and titanite (Fig. 3). Ilmenite, the main Ti-bearing mineral, displays a range of abundances and textural features in different samples. Classification of samples in this study is based on the whole-rock element compositions (see below). In the high-Mg/low-Ti series (groups 1 and 2), ilmenites

are present only as small grains in the groundmass (Fig. 3a-b). In the low-Mg/high-Ti series (group 3 and 4), they are present both in the groundmass and as phenocrysts in group 4 (Fig. 3e), but distinctly form extensive large clusters (glomerocrysts) in group 3 (Fig. 3c-d). Like other diabases within the Tethyan Himalaya (Zeng et al., 2016), the Dala diabase has undergone low-degree metamorphism and low-temperature alteration, expressed petrographically by the presence of hornblende, chlorite, and epidote replacing clinopyroxene with fish-shaped deformation (Fig. 3a-b); albite, biotite, and titanite embaying ilmenite margins (Fig. 3d-f); and minor quartz and pyrite.

3. SUMMARY OF ANALYTICAL METHODS

Zircons grains from two samples (T0766-1 and T0766-8) were selected for U-Pb dating and *in situ* zircon Hf isotope analysis. All diabase samples were analyzed for whole-rock elemental compositions and some typical samples were selected for Rb-Sr and Sm-Nd isotopic analysis. The major element compositions of Fe-Ti oxides (ilmenite) in Dala samples were also measured. Details of the analytical methods and data are given in the Appendix Materials.

4. RESULTS

4.1 Age of Dala diabase intrusion

Zircons grains from two samples (T0766-1 and T0766-8) show similar textures. Most of the zircon grains are short to elongated prisms characterized by broad oscillatory growth zoning (Fig. A1), consistent with primary magmatic growth. These grains, in both samples, yield low to intermediate U (96-1091 ppm), intermediate to

high Th (283-5943 ppm), and high Th/U ratios (>2.95 and up to 5.05). In sample T0766-1, 18 analyses yield concordant $^{206}Pb/^{238}Pb$ ages with limited scatter ranging from 129.6±1.3 Ma to 133.8±1.3 Ma, giving a weighted mean age of 131.7±0.6 Ma (MSWD = 0.91) (Fig. 4a-b). Sample T0766-8 shows similar features and yields a weighted mean age of 132.7±0.5 Ma (MSWD = 0.94) (Fig. 4c-d). Broad oscillatory growth zoning, high Th/U ratios, and concordance indicate that these ages represent the timing of crystallization of the Dala diabase intrusion. These ages are similar to those from the Comei and Cona areas (Zhu et al., 2009) and are entirely consistent with inclusion of the Dala diabase intrusion in the ~132 Ma Comei-Bunbury LIP.

In addition to those zircon grains described above, there are a few zircon grains with different textures (Fig. A1) that yield substantially older ages ~190 Ma (Table A1). These are presumed to represent captured xenocrysts during magma ascent.

4.2 Whole rock major and trace element geochemistry

TiO_2 content and Ti/Y ratio have long been viewed as important parameters to reflect the geochemical characteristics of mafic rocks (Peate et al., 1992; Xu et al., 2001 & 2004; Ren et al., 2017). In terms of whole-rock TiO_2 and MgO contents, the Dala diabase can be subdivided into two series: a high-Mg/low-Ti series and a low-Mg/high-Ti series (Fig. 5a). The distinction between these two series is also evident in a plot of Ti/Y against MgO contents (Fig. 5b), with the high-Mg/low-Ti series showing nearly constant Ti/Y whereas the low-Mg/high-Ti series shows a steep trend of variable Ti/Y. The substantial differences between the two series in major and trace element characteristics are described below.

High-Mg/low-Ti series: This series is characterized by high MgO (6.2-13.2 wt%), and CaO (7.6-9.9 wt%), but low TFeO (total Fe as FeO) (9.0-10.6 wt%), TiO_2 (1.5-2.4 wt%), and P_2O_5 (0.2-0.3 wt%). $Mg^{\#}$ (molar MgO/(MgO+TFeO)) values are high (53-70). Among compatible trace elements, this series shows high Cr (231-1129 ppm), Ni (45-176 ppm), and Co (33-65 ppm) but low V (215-294 ppm) contents. With decreasing MgO content, both SiO_2 and Al_2O_3 contents increase (Fig. 6a-b) while compatible elements Cr, Co and Ni decrease (Fig. 7a-c); all these features are generally consistent with evolution of liquid compositions by fractional crystallization of mafic minerals. The high-Mg/low-Ti series can be further subdivided into two groups. In group 1, as MgO content drops gradually, TFeO drops steeply while CaO, TiO_2, P_2O_5, and V are essentially constant, possibly due to fractional crystallization of olivine (Figs. 6c-f & 7d). In contrast, as MgO decreases, group 2 rocks show nearly constant TFeO, decreasing CaO, and increasing TiO_2, P_2O_5 and V. These features resemble the liquid line of descent expected for fractional crystallization of olivine and clinopyroxene together.

Low-Mg/high-Ti series: This series is characterized by low MgO (3.0-5.0 wt%), CaO (6.0-8.7 wt%), and $Mg^{\#}$ values (32-45), but high TiO_2 (2.8-4.6 wt%), TFeO (10.1-12.5 wt%), and P_2O_5 (0.3-0.5 wt%) contents (Fig. 6). Compatible trace elements show low Cr (2-17 ppm), Ni (5-20 ppm), and Co (30-38 ppm) but high V (322-461 ppm) contents (Fig. 7). SiO_2 increases gently while TiO_2 shows large variations over a small range in MgO (Fig. 6a & d). The low-Mg/high-Ti series also further subdivides into two groups. Group 3 has nearly constant MgO (4.4-5.0 wt%), P_2O_5, and SiO_2 but

a wide range of TFeO, TiO_2, CaO, Al_2O_3 and V contents (Figs. 6 & 7). In contrast, group 4 shows a more significant range in MgO correlated with substantial decrease in CaO and Al_2O_3 contents, gently decreasing TiO_2 content, and strongly increasing TFeO and P_2O_5 contents as MgO decreases (Fig. 6). Compared with the abnormal variations in group 3, trends in group 4 form continuous major element variations from high-Mg/low-Ti series and clear evidence of the onset of fractionation of plagioclase.

The behaviors of trace elements concentrations in the Dala diabase samples divide into the same series and groups as the major elements. Though total REE contents in the low-Mg/high-Ti series are higher than those in the high-Mg /low-Ti series, both series have similar REE patterns (Fig. 8a), somewhat enriched in light rare earth elements (LREE) relative to heavy rare earth elements (HERE) with La/Yb ratios ranging from 6.8 to 9.2 (Fig. 7f). There are only very minor negative Eu anomalies (Eu/Eu^*=0.89-1.00). Both series are enriched in LILEs (Rb, Th, U, K, Pb) relative to HFSEs (Nb, Ta, P) (Fig. 8b). However, some LILEs (e.g. Rb, Ba, K) show irregular negative anomalies in some high-Mg/low-Ti samples (Fig. 8b). Compared with the high-Mg/low-Ti series, the low-Mg/high-Ti series yields higher incompatible element contents (except for Rb and Sr) and only the low-Mg/high-Ti series shows weak positive Zr and Hf anomalies. Ti/Y ratios for high-Mg/low-Ti series keep almost constant (373-426), but show large variations for low-Mg/high-Ti series (306-696) (Fig. 5b). Ce/Pb (4.4-13.3) and Nb/U (9.3-13.3) ratios of both series are close to those of island arc basalts and clearly distinct from mid-ocean ridge basalts or ocean island

basalts (Fig. 9b, Hofmann et al., 1986). Incompatible element ratios are similar for members of the two suites: Nb/Ta is 12.9-14.9 for the low-Mg/high-Ti series and 12.6-14.3 for the high-Mg/low-Ti series, whereas Zr/Hf is 38.4-45.9 for the low-Mg/high-Ti series and 34.9-41.3 for the high-Mg/low-Ti series.

4.3 Sr and Nd isotope compositions

Sr and Nd isotopic data for 15 whole rock samples of the Dala diabase intrusion are listed in Table A3. A value of T = 132 Ma was assigned to calculate the initial Sr and Nd isotopic compositions. The initial isotopic compositions of analyzed samples are graphically presented on an $\varepsilon_{Nd}(t)$ versus $^{87}Sr/^{86}Sr(t)$ diagram (Fig. 10). All the data points on this plot have analytical uncertainties smaller than the plotted symbols. The Dala diabases have low Rb (< 85 ppm) but high Sr (> 151 ppm), Sm (> 4.0 ppm), and Nd (> 18.0 ppm) contents, which result in low Rb/Sr (< 0.35) and Sm/Nd (< 0.26) ratios. Except for one sample, T0766-1, that has depleted initial isotope compositions ($^{87}Sr/^{86}Sr(t)$ = 0.7050, $\varepsilon_{Nd}(t)$ = +6.1), most samples of both series, regardless of their MgO contents, show uniform weak enrichment characteristics ($^{87}Sr/^{86}Sr(t)$ = 0.7065-0.7075, $\varepsilon_{Nd}(t)$ = −2.8-−1.5). Two samples (T0766-10 and T0766-11) are characterized by elevated $^{87}Sr/^{86}Sr(t)$ (0.7087, 0.7089) but similar $\varepsilon_{Nd}(t)$ values (−1.5, −0.7) compared to the other samples. As Sr abundance and isotope ratios are highly sensitive to alteration and low-grade metamorphism, we interpret these anomalously high initial Sr isotope ratios as reflecting post-magmatic processes.

4.4 Zircon Hf isotope compositions

The zircon Hf isotope analytical results for samples T0766-1 and T0766-8 are

listed in Table A2 and shown graphically in Fig. 11. Sample T0766-1 zircons show a continuous distribution of $\varepsilon_{Hf}(t)$ values from +10.5 to +14.3 with a weighted mean value of 12.3±0.6 (MSWD = 1.9, n=16) (Fig. 11a). This mean is fully consistent with the depleted whole-rock Nd isotopic compositions of this sample ($\varepsilon_{Nd}(t)$ = +6.1). On the other hand, sample T0766-8 zircons show a continuous and statistically homogeneous distribution of $\varepsilon_{Hf}(t)$ values from −2.6 to +0.6 with a weighted mean value of −1.1±0.5 (MSWD = 0.94, n=16) (Fig. 11b). Although this sample was not measured for Nd isotopes, the zircon Hf isotope signature is consistent with the weakly enriched whole-rock Nd isotopic compositions ($\varepsilon_{Nd}(t)$ = −2.8-−0.7) of all the samples except T0766-1. One, presumably inherited, zircon grain (T0766-8-5.1) that yielded an anomalously old U-Pb age (~190 Ma) has $\varepsilon_{Hf}(t)$ value of +14.0 (Table A2) and a crustal model age (t_{DM1}) of 236 Ma.

4.5 Ilmenite electron microprobe analyses

Although the sizes and petrographic textures of ilmenite grains vary among different groups, the major element compositions of ilmenite from all groups in this study are homogeneous and nearly identical in TiO_2 (52.29-53.30 wt%), FeO (44.91-45.85 wt%) and MnO (1.50-2.30 wt%) contents. Petrographic observations and EPMA data both indicate that ilmenite is the dominant phase hosting the whole-rock budget of Ti. The MgO content of ilmenite from the high-Mg/low-Ti series (0.09-0.21 wt%) is higher than that of the low-Mg/high-Ti series (0.02-0.11 wt%), consistent with the whole-rock MgO content variations of samples in this study.

5. DISCUSSION

5.1 Effects of post-magmatic alteration and low-grade metamorphism on elemental mobility

The common secondary phases, including hornblende, chlorite, epidote, albite and titanite, found by petrographic observations (Fig. 3) indicate that the Dala diabases have experienced hydrothermal alteration and greenschist facies metamorphism since emplacement. Both olivine and pyroxene have been almost completely replaced by hornblende, chlorite, and epidote.

However, the major element contents for all Dala samples, except for group 3, form continuous variations in all oxide variations diagrams, continuing from the high-Mg/low-Ti series through the low-Mg/high-Ti series (Fig. 6), suggesting that trends in whole-rock chemistry generated by magmatic differentiation have been largely preserved through metamorphism and alteration. In addition, all samples have LOI values less than 2.3 wt% that do not show obvious correlations with the major elements, which discounts the idea that apparent fractionation trends were created by metasomatic alteration whose intensity was a systematic function of MgO. Therefore, the major elements of the Dala samples in this study are considered to have been rather little modified by hydrothermal alteration or metamorphism. Possible exceptions include Ca and Na, potentially mobile elements whose variation in the Dala suite is difficult to explain if CaO and Na_2O concentrations are truly primary.

A general consensus exists that during hydrothermal alteration or low-grade metamorphism, LILEs (e.g., Rb, Ba, K, Na, Sr) can be remobilized, whereas transition metals (e.g., Cr, Ni), REEs, HFSEs, Th and Ti in mafic rocks are relatively

immobile (Smith and Smith, 1976; Ludden and Thompson, 1978; Bienvenu et al., 1990; Staudigel et al., 1996). This could explain the observation (Fig. 8b) that some LILEs (e.g., Rb, Ba and K) show irregular variations, likely due to post-magmatic alteration. Apart from these specific fluid-mobile elements, the samples in both series of Dala diabases have subparallel patterns on both REE and extended trace element diagrams (Fig. 8). The immobile elements also do not show any correlation with LOI. We therefore conclude that the diabase samples of this study still preserve, at the level of precision of our analyses and plots, their original REE and trace element signatures. We will proceed to use the fluid-immobile elements, including transition metals (e.g., Cr, Ni), HFSEs (Ti, Nb, Ta, Zr, Hf), Th, and REEs, to constrain magmatic processes and geochemical sources for these diabases.

5.2 Nature of the mantle source for the Dala diabase rocks

The Dala diabase is located at the southeastern margin of the Yardoi gneiss dome and formed at ~132 Ma, contemporaneous with regional mafic rocks that have been grouped into the early Cretaceous Comei-Bunbury LIP (Fig. 1, Zhu et al., 2009). Previous studies have demonstrated that the Comei-Bunbury LIP represents mafic magmatism associated with the break-up of the Eastern Gondwana continent due to impingement of the Kerguelen plume (Zhu et al., 2007 & 2009; Liu et al., 2015). Literature data also show that ~132 Ma mafic members of this LIP to the south and west of Dala are characterized by slightly more unradiogenic Nd ($\varepsilon_{Nd}(t)$ = +1.6-+4.3) and radiogenic Sr ($^{87}Sr/^{86}Sr(t)$ = 0.7040-0.7070) isotopic compositions and higher Nb/La (> 0.75) ratios (Zhu et al., 2007 & 2008; Xia et al., 2014; Liu et al., 2015) than

lavas derived directly from depleted mantle sources. Such isotopic compositions are in the range of many OIB worldwide, as summarized by White (2015).

Within the Dala pluton, except for one sample (T0766-1) with relatively high Nd and Hf isotope compositions, all the other samples, regardless of their MgO and TiO_2 contents, are characterized by substantially lower $\varepsilon_{Nd}(t)$ (< −1.6), elevated $^{87}Sr/^{86}Sr(t)$ (> 0.7066) ratios, and lower Nb/La (< 0.56) ratios (Fig. 10), suggesting involvement of a different and more enriched component that mixed with Kerguelen plume-derived melts in the source of the Dala mafic rocks. Other lines of evidence that indicate and help to fingerprint the crust-like component in the Dala diabases include (1) substantial negative Nb and Ta anomalies and positive Pb anomalies (Fig. 8b), (2) high $(La/Nb)_{PM}$ and $(Th/Nb)_{PM}$, and (3) low Ce/Pb and Nb/U ratios (Fig. 9).

The geochemical signature of such a crust-like component is also apparent in the contemporary Bunbury Gosselin lavas in Australia (Frey et al., 1996), in ~116 Ma Group II Rajmahal (Kent et al., 1997) and Sylhet Traps (Ghatak and Basu, 2011) and in lavas that are part of the Kerguelen Plateau (ODP Site 738 on southern Kerguelen Plateau), as summarized in Fig.10b. However, there is no consensus on the geochemical compositions or origin of the enriched component observed in the products of Kerguelen plume activity, with various authors arguing for upper crust, lower crust, and subcontinental lithospheric mantle (Frey et al., 1996 & 2002; Kent et al., 1997; Ghatak and Basu, 2011 & 2013).

Most Dala samples show relatively uniform $\varepsilon_{Nd}(t)$ (−2.8-−0.7) and Nb/La (0.42-0.56) values, even including the high-Mg/low-Ti suite, and no correlation of

$\varepsilon_{Nd}(t)$ with MgO or SiO_2 contents. Similar crust-like isotopic signatures were also found in the ~140 Ma Kerguelen plume-related high-Mg diabase rocks in the Gyangze area, south Tibet (Wang et al., 2016, Fig.1C). These observations strongly suggest that this crust-like signature was inherited from one relatively homogeneous deep source, and not from a progressively assimilated upper crustal contaminant during magma ascent and differentiation. Considering the high Mg contents in several Dala samples, the most likely candidate for this enriched component is the overlying Greater India subcontinental lithospheric mantle (SCLM), which acquired its geochemical signature through metasomatism by fluids or low-degree melts. The early Cretaceous (~117-118 Ma) Rajmahal-Sylhel basalts in eastern India are widely viewed as products of the Kerguelen plume activities (Mahoney et al., 1983; Kent et al., 1997; Frey et al., 2002; Ghatak and Basu, 2011). In the eastern and northeastern India, a variety of contemporaneous alkaline-carbonatitic complexes (such as Sung Valley, Jasra, Samchampi) and ultrapotassic intrusive rocks, located close to the exposed Rajmahal-Sylhel basalts, in the Shilong Plateau and Damodar Valley, provide significant evidences to explore the geochemical characteristics of Greater India subcontinental lithospheric mantle (Srivastava et al., 2005; Srivastava and Sinha, 2007; Melluso et al., 2012; Chalapathi Rao et al., 2014). Above rocks with largely variable $^{87}Sr/^{86}Sr(t)$ (0.7046-0.7104) and $\varepsilon_{Nd}(t)$ ($+0.7$--12.8) compositions (Fig.10b) have been viewed as products of the mantle-derived magmas from melting of highly isotopically heterogeneous lithospheric mantle (Melluso et al., 2012), which underwent multiple episodes of mantle metasomatism (Srivastava et al., 2005;

Melluso et al., 2012; Chalapathi Rao et al., 2013 a, b & 2014). Assumping that the enriched component in the Dala diabase source is derived from the most enriched metasomatized part of Greater India SCLM ($^{87}Sr/^{86}Sr(t)$=0.7104; $\varepsilon_{Nd}(t)$=−12.84) inferred by alkaline samples from Sung Valley (Srivastava et al., 2005), only small amount incorporation of this SCLM-derived melting in the Kerguelen plume-derived melts can be responsible for the Sr-Nd isotopic compositions of most Dala samples, consistent with the absence of obvious mixing effects on major oxide concentration (e.g. MgO, SiO_2). Therefore, the Dala diabase likely represents products generated by the Kerguelen starting plume mixed with a small mass fraction of the enriched component from subcontinental lithospheric mantle in Greater India, which model is common in may LIPs (Baker et al., 1997; Lassiter and DePaolo, 1997; Simonetti et al., 1998; Xiao et al., 2004; Said et al., 2010).

Returning to the unique sample T0766-1 that shows relative depleted zircon Hf isotope ($\varepsilon_{Hf}(t)$ = +10.5-+14.3) and whole-rock Nd isotope ratios ($\varepsilon_{Nd}(t)$ = +6.1), we note that its Nd isotopic compositions are consistent with the a number of Kerguelen plume products with equally high $\varepsilon_{Nd}(t)$, including parts of the Ninety-Eastern Ridge and Kerguelen Plateau (Fig.10b). However, the crust-like Nb-Ta-Ti depletion of sample T0766-1 resemble other Dala samples still suggest enriched component in the source of this rock. This unique sample can be explained by the interaction between the Kerguelen plume-derived melts with a small mass fraction of the relatively less enriched subcontinental lithospheric mantle component from Greater India, which is also consistent with the clear heterogeneities in early Cretaceous subcontinental

lithospheric mantle in northeastern India (Melluso et al., 2012 and Fig. 10b).

5.3 Magmatic evolution model of the Dala diabase: major elements

A number of flood basalt provinces (e.g., the Paraná, the Karoo and the Emeishan basalts) host contemporaneous high-Ti and low-Ti basaltic magmas (Cox et al., 1967 & 1988; Gibson et al., 1995 & 1996; Xu et al., 2001 & 2004; Ren et al., 2017). The Dala diabase pluton also hosts high-Ti and low-Ti series rocks. Despite the distinct major and trace element compositions of the two suites of rocks, they occur in close spatial and temporal proximity and share similar Nd isotope compositions and parallel REE distribution patterns with smoothly changing overall abundances. These features are all consistent with a co-genetic origin for two suites, which motivates the investigation of the petrogenetic process by which the whole pluton may have evolved from a common source.

Most major element correlations are continuous through both series (Fig. 6) and are qualitatively of the sense expected for common fractional crystallization processes. In particular, with the possible exception of Group 3 from the low-Mg/high-Ti suite, the correlated variations in TiO_2 and MgO (Fig. 6d) are broadly consistent with a single liquid line of descent (LLD) rather than two distinct parental magmas. The high-Mg/low-Ti suite, dominantly rocks with MgO > 8.0 wt%, represents more primitive melts that, like most common primary mafic magmas, are undersaturated in TiO_2 and other Ti-rich phases (Hellman and Green, 1979; Ryerson and Watson, 1987; Hess, 1992; Prytulak and Elliott, 2007). Within the high-Mg/low-Ti series, there are approximately linear decreasing trends against MgO in elements such as Cr, Co, and

Ni (Fig. 7) that are compatible in mafic minerals.

Curiously, Group 1 shows sharply decreasing TFeO and nearly constant CaO, TiO_2 and P_2O_5, whereas Group 2 is marked by declining CaO and increasing TiO_2 and P_2O_5 at near constant TFeO (Fig.6). There appear to be two distinct fractionating mineral assemblages within the series. Group 1 is dominated by segregation of low-Ca mafic phases such as olivine or orthopyroxene, where Group 2 reflects early removal of high-Ca mafic phases such as clinopyroxene. The divergence of evolution paths from an apparently common source poses a challenge for differentiation models, requiring differences in imposed conditions of fractionation or controls on chemistry other than ordinary fractional crystallization along a liquid line of descent.

The low-Mg/high-Ti series, especially Group 4, with low MgO, CaO, Cr, Co, Ni and high TFeO, TiO_2, P_2O_5 (Figs. 6 & 7), resembles the residual liquid expected from continuing fractional crystallization along the path of Group 2 of the high-Mg/low-Ti series. The sharp break in slope on many variation diagrams at ~5 wt% MgO suggests a major change in fractionating phase assemblage. Decreasing Al_2O_3 and CaO combined with steeply increasing SiO_2, TFeO, and P_2O_5, point to a large proportion of plagioclase in the fractionating assemblage beyond this point (Figs. 6 & 7). If this is the case, then the failure to develop a large Eu anomaly requires oxidizing conditions during plagioclase fractionation, keeping most of the Eu in the 3+ state. Although it is tempting to associate the apparent decrease in TiO_2 contents with MgO in Group 4 with onset of Fe-Ti oxide fractionation, this is not consistent with continuing increase in total FeO and it is difficult to achieve either magnetite or ilmenite saturation at this

point in quantitative models (see below). Moreover, Group 3 displays a number of discontinuities from the variation sequence of the other samples (e.g. in total FeO, TiO_2, V, and Co) that are quite difficult to achieve if these samples represent liquid compositions along the same liquid line of descent as the other samples. A component of some other magmatic process must be invoked to explain the detailed compositions of Group 3.

In order to provide more details on the fractionating processes indicated by these composition trends, we model the relationships using the alphaMELTS implementation (Smith and Asimow, 2005) of the MELTS thermodynamic model (Ghiorso and Sack, 1995). A fractionation model must begin either from the most primitive observed sample or from an estimated primary magma. Because lavas with high MgO and CaO contents consistent with partial melting of a peridotite source can be used to constrain primary magma compositions and melting conditions (Herzberg and Asimow, 2015), we adopt the strategy of estimating a primary magma composition as a starting point for our fractionation models. The most primitive sample (T0766-1) is suitable for primary magma calculation by PRIMELT3 modeling and yields a successful primary magma solution with 48.5 wt% SiO_2, 16.0 wt% MgO, 9.6 wt% CaO, 1.5 wt% TiO_2, melt fraction of 0.29, and potential temperature of 1461 ^{o}C. We studied the sensitivity of model fractional crystallization pathways beginning with this modeled primary magma to variable pressures (3000 bars and 5000 bars) and oxygen fugacity buffers (QFM+1 and QFM−1). Initial H_2O content was held at 0.1 wt%. Among the three fractional crystallization pathways shown in Fig. 6, Dala

samples, with the exception of Group 3 in the low-Mg/high-Ti suite, are mostly consistent with the single liquid line of descent at 3000 bars and QFM+1, especially in terms of SiO_2, TFeO and P_2O_5 contents. The crystallization sequence in this model is olivine, orthopyroxene, spinel, clinopyroxene, plagioclase, and finally ilmenite and apatite. These modeling results confirm a relatively high oxygen fugacity condition (QFM+1) during the magmatic differentiation process.

However, some obvious deviations, significantly larger than analytical uncertainty require the action of other evolutionary processes. First, the fractionation model at 3000 bars with QFM+1 does not give enough high-Fe olivine fractionation to explain the obvious decreasing TFeO trends in group 1, which may call for low oxygen fugacity condition (QFM−1) as shown in Fig. 6c. In addition, several samples with low CaO contents from group 2 (Fig. 6e) and several samples with low Al_2O_3 contents from group 3 and 4 (Fig. 6b) do not plot on any of the calculated liquid lines of descent. If not due to post-magmatic alteration effects (Staudigel et al., 1996), mixing of primitive and evolved magmas offers a plausible explanation for samples plotting within the field of concavity of the calculated liquid lines of descent.

The group 3 samples, with especially large ranges of TiO_2 and TFeO contents and Ti/Y ratios, plainly deviate from the variation sequence of the model liquid line of descent in Fig. 6. From petrographic observations, the much higher proportions of ilmenite and presence of glomerocrysts only in group 3 indicates a potential accumulation process. Yet, the modeled liquid lines of descent reveal that none of the Dala samples are evolved enough to capture the late stages of fractionation where

Fe-Ti oxide sequestration causes TFeO and TiO_2 to decrease sharply (Fig. 6). It is a puzzle to find accumulation of ilmenite in group 3 when the observed suite does not include bulk compositions evolved enough to have been crystallizing Fe-Ti oxides. Considering the high density contrast between ilmenite and residual melt, one plausible origin for the observed ilmenite grains and Ti-enrichment would be a vertically zoned magma chamber with more evolved magmas crystallizing ilmenite at a high level, now eroded or unexposed. Dense clusters of ilmenite formed in these high-level evolved liquids could settle rapidly and subside downwards into the more primitive liquids that eventually formed the group 3 rocks. Such settled ilmenite clusters would be out of equilibrium with their host rocks, which is consistent with the titanite reaction rims observed (Fig. 3f). The mechanism of ilmenite sorting due to gravity-induced subsidence has been found in the world-class Tellnes ilmenite deposit, SW Norway, and is viewed as one important ilmenite enrichment mechanism (Charlier et al., 2006 & 2007). As a result, we propose that the ilmenite clusters in group 3 were most likely formed in a higher, cooler part of the magma chamber and subsequently settled into the deeper layer represented by group 3. This settling was accompanied by some resorption as well as clustering of ilmenite grains. The *MELTS* modeling results indicate that continuing fractionation along the modeled liquid line of descent indeed should form ilmenite with composition similar to that observed in the EPMA data, with 47-51 wt% TiO_2 and 39-45 wt% TFeO.

In summary, we are able to explain, for the most part, the variation in the composition within the Dala suite in terms of magma differentiation processes. The

presence of a range of TiO_2 contents within this pluton therefore argues against a simple use of TiO_2 in mafic magmas as an indicator of the mantle source without due consideration of the influence of magmatic differentiation.

5.4 Magmatic evolution of the Dala diabase - trace elements

The major element evidence shows that a variety of fractionating phases and possibly other processes influenced the evolution of the Dala diabase. Many of the same features can be recognized in the trace elements.

Compatible elements such as Cr, Ni, and Co have relatively large mineral/melt partition coefficients in olivine and pyroxene (Rollinson, 1993; Nielsen et al., 1992). Indeed, these elements show a positive and mostly linear relationship with MgO in the high-Mg/low-Ti series (Fig. 7), consistent with removal of fractionating olivine and/or pyroxenes. The "step" in the Ni trend in Group 2 might reflect a peritectic change from olivine to pyroxene crystallization. By the time differentiation reaches the compositions of the low-Mg/high-Ti series, these elements have mostly been removed from the liquid, consistent with the low observed concentrations (Fig. 7). The mineral/melt partition coefficients of V between basaltic liquids and mafic minerals, especially iron-rich minerals, are mainly controlled by the oxygen fugacity conditions (Canil, 1999; Toplis and Corgne, 2002). V concentrations are positively correlated with TiO_2 contents in all Dala samples (Fig. 7e) and negatively correlated with MgO (Fig. 7d), except for Group 3. V and Ti are both behaving as incompatible elements, becoming enriched in the residual liquid during fractional crystallization, suggesting a relatively high fO_2 condition to stabilize high valence states of V and keep it

incompatible in mafic phases (Mallmann and O'Neill, 2009 & 2013). The anomalous dramatically increasing behavior of V in Group 3 (Figs. 7d) is consistent with the ilmenite accumulation process invoked above to explain the TiO_2 contents.

The partitioning behaviors of REEs can also yield key insights into magma evolution history. The nearly parallel REE patterns with gradually increasing LREE/HREE slope (Fig. 7f) of the whole suite are consistent with gradual enrichment in residual liquid, and the absence of Eu anomalies in the low-Mg/high-Ti suite are consistent with oxidizing conditions that stabilize mostly Eu^{3+}. The total concentrations of REEs in the Dala diabases are very well positively correlated with whole-rock P_2O_5 contents (Fig. 7h), suggesting that the REEs behave similarly to P and that apatite is the main REE-bearing phase. The trace element (Cr, Co, Ni, V, and REEs) model result from alphaMELTS according to the fractionation model derived for major elements at 3000 bars and QFM+1 with 0.1 wt% initial H_2O also provides a good fit to the Dala trace element data (Fig. 7).

The high-Mg/low-Ti series are characterized by nearly constant Ti/Y (373-426), in contrast with great variations (306-696) in the low-Mg/high-Ti series (Fig. 5b). Such distinct variations in Ti/Y between these two series could also be explained by magma evolution. Element Y, as one of the HREEs, is positively correlated with P_2O_5. TiO_2 and P_2O_5 contents both show gently increasing trends during the early stage of magma differentiation (the high MgO stage, Fig. 6d & f), which leads to almost constant Ti/Y ratios in the high-Mg/low-Ti series. However, in the later stages of differentiation, TiO_2 begins to decrease significantly earlier than P_2O_5 (or Y) because

Fe-Ti oxides begin to crystallize before apatite saturation, as indicated by the *MELTS* simulation results (the low MgO stage, Fig. 6d & f). The combination of decreasing TiO_2 and increasing P_2O_5 and Y give the obvious decreasing Ti/Y ratios of group 4 (Fig. 5b). Likewise, the steep trend in Ti/Y ratios in group 3 can be attributed to accumulation of ilmenite into magmas not yet saturated in apatite boosting TiO_2 contents significantly but contributing little to Y concentrations.

5.5 Implications for the magmatic evolution of the Comei LIP

Numerous isotopic and geochemical studies have shown that most large igneous provinces and ocean island groups involve two or more components, on both global and regional scales. These components include primitive mantle, depleted mid-ocean ridge basalt mantle (DMM), sub-continental lithospheric (SCLM), and perhaps recycled continental/oceanic crust, pelagic sediment, or even outer core material (Ellam et al., 1992; Horan et al., 1995; Walker et al., 1995, 1999, 2002; Bennett et al., 1996; Hofmann, 1997; Sobolev et al., 2005 & 2007; Jackson et al., 2006, 2008, 2012). Although the mafic rocks defining the Comei LIP are generally thought to be produced by activity of the Kerguelen mantle plume, the origin and geochemical structure of the Kerguelen mantle plume over the course of its lifetime still remain unclear and the magmatic characteristics of the Comei LIP can help to resolve questions concerning the evolution of the Kerguelen mantle plume.

Literature data summarized in Figs. 1 and 10 indicate that magmatic rocks associated with the Kerguelen mantle plume are dominantly mafic diabase dikes and basaltic lavas, with sparse evolved samples ranging from alkaline diorite to granitoids.

The silicic rocks, with negative $\varepsilon_{Nd}(t)$ values from –11.6 to –11.0 (Fig. 10), are interpreted to be silicic melts derived from anatexis of shallow crustal materials, triggered by heat input from the Kerguelen mantle plume (Zhu et al., 2007; Liu et al., 2015). In contrast, most of the mafic rocks represent mantle-derived magma. Excluding those altered samples with anomalous elevated initial Sr isotopic compositions, the majority of mantle-derived rocks from the Comei LIP can be divided into three end-members (Fig. 10). (1) A mantle plume end-member characterized by OIB-like REE and trace element patterns with $\varepsilon_{Nd}(t)$ values from +1.6 to +4.3, $^{87}Sr/^{86}Sr(t)$ values from 0.7040 to 0.7070, absence of Nb-Ta anomalies, and roughly chondritic Nb/La values from 0.76 to 1.11 (Zhu et al., 2007 & 2008; Xia et al., 2014; Liu et al., 2015) is widely distributed in the Comei LIP, including the Cona, Rimowa and Gyangze areas (Fig. 1). (2) A plume-SCLM mixing end-member characterized by subduction influenced trace element patterns with obvious negative Nb-Ta anomalies, low Nb/La from 0.42 to 0.68, relatively low $\varepsilon_{Nd}(t)$ values from –3.3 to –1.5, and high $^{87}Sr/^{86}Sr(t)$ values from 0.7066 to 0.7075 has been documented in the Gyangze areas and dominates the Dala pluton (Fig.1, Wang et al., 2016 and this paper). The geochemistry of this end-member is consistent with mixing in reasonably constant proportions between (dominantly) Kerguelen plume-derived melts and (minor) melts derived from the enriched early Cretaceous Greater India subcontinental lithospheric mantle. Finally, (3) A depleted end-member characterized by N-MORB-like REE distribution patterns with $\varepsilon_{Nd}(t)$ values from +5.7 to +6.4, $^{87}Sr/^{86}Sr(t)$ values from 0.7050 to 0.7060, and intermediate Nb/La ratios from 0.51 to

0.63 are relatively scarce, located only in the Cona area (Fig. 1), and are interpreted as melts derived from depleted asthenospheric mantle (Zhu et al., 2008). Collectively, the new data presented here and those from the literature both demonstrate that the source regimes for the mafic rocks in the Comei LIP show continuity over time in the geochemical character of the Kerguelen plume, with similar components found in the Rajmahal and Sylhet Traps, along the Ninety-Eastern Ridge and Broken Ridge, and throughout the Kerguelen Plateau and Islands themselves (Figs. 1 & 10).

After attempting to correct for variability of Ti due to magmatic differentiation, previous studies have proposed that the Ti contents as well as Ti/Y ratios and the distribution patterns of high-Ti versus low-Ti mafic rocks in LIPs can be used as a proxy to infer sources characteristics and the structure of a mantle plumes (Cox et al., 1967 & 1988; Gibson et al., 1995 & 1996; Xu et al., 2001 & 2004). However, we show here that the Ti contents in the Dala diabase are controlled dominantly by magmatic evolution processes rather than the mantle sources. The distribution of high-Ti (TiO_2 > 2.5 wt%) and low-Ti (TiO_2 < 2.5 wt%) mafic rocks throughout the Comei LIP does not show any systematic spatial pattern (Fig. 1). Both suites of rocks coexist in most localities. Except for a few depleted end-member samples with markedly low Ti content, mafic rocks throughout this LIP, whether isotopically close to the mantle plume end-member or to the plume-SCLM mixing end-member, include both high-Ti and low-Ti rocks. TiO_2 by itself in the whole group and within each geochemical subgroup is uncorrelated with either $\varepsilon_{Nd}(t)$ or Nb/La ratio (Fig. 12a-b). Samples from the two end-members throughout the Comei province generally

resemble the typical liquid line of descent for a primary OIB composition in Fig.12c (Prytulak and Elliott, 2007), indicating major control by magmatic differentiation. Hence, elemental Ti and Ti/Y ratio variations in Comei LIP and other magmatic provinces cannot – *by themselves* – be used to infer the nature of their sources. It is necessary to correct for fractionation by examining data in TiO_2-MgO space before drawing such inferences.

6. Conclusion

The Dala diabase, formed at ~132 Ma, is part of the Comei LIP, the products of melting of dominantly Kerguelen plume-derived melts mixed minor melts derived from the enriched early Cretaceous Greater India subcontinental lithospheric mantle. The Dala diabase consists of a high-Mg/low-Ti series and a low-Mg/high-Ti series of mafic rocks, although both suites share a common isotopic character and systematically related trace element signature. The high-Mg/low-Ti series are more primitive mafic magmas and lie on a common liquid line of descent with most of the low-Mg/high-Ti suite, dominated by olivine and clinopyroxene fractionation, followed by plagioclase within the low-Mg/high-Ti series. These processes also lead to systematic changes in trace element geochemistry, especially in compatible elements, REE, and major elements such as Ti and P. However, a subgroup of the low-Mg/high-Ti suite displays an anomalous trend in major and trace-element variation that may show ilmenite accumulation rather than magmatic liquid compositions. We show that consideration of the petrogenetic relationship between low-Ti and high-Ti mafic rocks, for example in TiO_2-MgO space, is necessary before

using Ti contents to infer the structure of source regimes or degrees of melting.

Acknowledgements

This study was supported by Special Scientific Research Fund of Public Welfare Profession of China (Grant No.201511022), China Geological Survey Project (Grant No.12120115027101), National Science Foundation of China (Grant Nos.41425010, 41503023) and National Foundation from China Scholarship Council. PDA's participation was supported by the US National Science Foundation, award EAR-1550934.

REFERENCES

Aikman, A.B., Harrison, T.M., Lin, D., 2008. Evidence for Early (>44 Ma) Himalayan Crustal Thickening, Tethyan Himalaya, southeastern Tibet. Earth and Planetary Science Letters 274, 14-23.

Baker, J.A., Menzies, M.A, Thirlwall, M.F., MacPherson, C.G., 1997. Petrogenesis of Quaternary intraplate volcanism, Sana'a, Yemen: implications for plume-lithosphere interaction and polybaric melt hybridization. Journal of Petrology 38, 1359-1390.

Bennett, V.C., East, T.M., Norman, M.D., 1996. Two mantle-plume components in Hawaiian picrites inferred from correlated Os-Pb isotopes. Nature 381, 221-224.

Bienvenu, P., Bougault, H., Joron, M., Dmitriev, L., 1990. MORB alteration: rare-earth element/non-rare earth hygromagmaphile element fractionation. Chemical Geology 82, 1-14.

Bhat, M.I., 1984. Abor Volcanics: further evidence for the birth Tethys Ocean in the Himalayan segment. Journal of the Geological Society 141, 763-775.

Botcharnikov, R.E., Almeev, R.R., Koepke, J. Holtz, F., 2008. Phase relations and liquid lines of

descent in hydrous ferrobasalt-implications for the Skaergaard intrusion and Columbia River flood basalts. Journal of Petrology 49, 1687-1727.

Cai, F., Ding, L., Laskowski, A. K., Kapp, P., Wang, H., Xu, Q., Zhang, L., 2016. Late Triassic paleogeographic reconstruction along the Neo–Tethyan Ocean margins, southern Tibet. Earth and Planetary Science Letters 435, 105-114.

Canil, D., 1999. Vanadium partitioning between orthopyroxene, spinel and silicate melt and the redox states of mantle source regions for primary magmas. Geochimica et Cosmochimica Acta 63, 557-572.

Chalapathi Rao, N., Srivastava, R.K., Sinha, A.K., and Ravikant, V. 2014. Petrogenesis of Kerguelen mantle plume-linked Early Cretaceous ultrapotassic intrusive rocks from the Gondwana sedimentary basins, Damodar Valley, Eastern India. Earth-Science Reviews 136, 96-120.

Chalapathi Rao, N., Sinha, A.K., Kumar, S., and Srivastava, R.K. 2013a. K-rich titanate from the Jharia ultrapotassic rock, Gondwana coal fields, eastern India, and its petrological significance. Journal of the Geological Society of India 81, 733-736.

Chalapathi Rao, N., Wu, F.Y., Mitchell, R.H., Li, Q.L., and Lehmann, B. 2013b. Mesoproterozoic U–Pb ages, trace element and Sr–Nd isotopic composition of perovskite from kimberlites of the Eastern Dharwar craton, southern India: Distinct mantle sources and a widespread 1.1 Ga tectonomagmatic event. Chemical Geology 353, 48-64.

Chauvet, F., Lapierre, H., Bosch, D., Guillot, S., Mascle, G., Vannay, J.C., Cotton, J., Brunet, P., and Keller, F., 2008. Geochemistry of the Panjal Traps basalts (NW Himalaya): Records of the Pangea Permian break-up. Bulletin de la Société Géologique de France 179, 383-395.

Charlier, B., Duchesne, J.C., Vander, Auwera, J., 2006. Magma chamber processes in the Tellnes ilmenite deposit (Rogaland Anorthosite Province, SW Norway) and the formation of Fe–Ti ores in massif-type anorthosites. Chemical Geology 234, 264-290.

Charlier, B., Skår, Ø., Korneliussen, A., Duchesne, J.C., Auwera, J.V., 2007. Ilmenite composition in the Tellnes Fe–Ti deposit, SW Norway: fractional crystallization, postcumulus evolution and ilmenite–zircon relation. Contributions to Mineralogy and Petrology 154, 119-134.

Cox, K.G., MacDonald, R., Hornung, G., 1967. Geochemical and petrographic provinces in the Karoo basalts of southern Africa. American Mineralogist 52, 1451-1474.

Cox, K.G., 1988. The Karoo Province. In: Macdougall, J.D. (Eds.), Continental flood basalts, 239-271.

Dai, J.G., Yin, A., Liu, W.C., Wang, C.S., 2008. Nd isotopic compositions of the Tethyan Himalayan sequence in southeastern Tibet. Science in China Series D: Earth Sciences 51, 1306-1316.

Diedesch, T. F., Jessup, M. J., Cottle, J. M., Zeng, L.S., 2016. Tectonic evolution of the middle crust in southern Tibet from structural and kinematic studies in the Lhagoi Kangri gneiss dome. Lithosphere 8, 480-504.

Ellam, R.M., Carlson, R.M., Shirey, S.B., 1992. Evidence from Re-Os isotopes for plume-lithosphere mixing in Karoo flood basalt genesis. Nature 359, 718-721.

Ewart, A., Marsh, J. S., Milner, S. C., Duncan, A. R., Kamber, B. S., Armstrong, R. A., 2004. Petrology and geochemistry of Early Cretaceous bimodal continental flood volcanism of the NW Etendeka, Namibia. Part 2: Characteristics and petrogenesis of the high-Ti latite and high-Ti and low-Ti voluminous quartz latite eruptives. Journal of Petrology 45, 107-138.

Fodor, R. V., 1987. Low-and high-TiO_2 flood basalts of southern Brazil: origin from picritic parentage and a common mantle source. Earth and Planetary Science Letters 84, 423-430.

Frey, F.A., McNaughton, N.J., Nelson, D.R., Delaeter, J.R., Duncan, R.A., 1996. Petrogenesis of the Bunbury Basalt, Western Australia: interaction between the Kerguelen plume and Gondwana lithosphere? Earth and Planetary Science Letters 144,163-183.

Frey, F.A., Coffin, M.F., Wallace, P.J., Weis, D., Zhao, X., Wise Jr., S.W., Wahner, V., Teagle, D.A.H., Saccocia, P.J., Reusch, D.H., Pringle, M.S., Nicolaysen, K.E., Neal, C.R., Müller, R.D., Moore, C.L., Mahoney,J.J., Keszthelyi, L., Inokuchi, H., Duncan, R.A., Delius, H., Damuth, J.E., Damasceno, D., Coxall, H.K., Borre, M.K., Boehm, F., Barling, J., Arndt, N.T., Antretter, M., 2000. Origin and evolution of a submarine large igneous province: the Kerguelen Plateau and Broken Ridge, southern Indian Ocean. Earth and Planetary Science Letters 176, 73-89.

Frey, F.A., Weis, D., Borisova, A.Y., Xu, G., 2002. Involvement of continental crust in the formation of the Cretaceous Kerguelen Plateau: new perspectives from ODP Leg 120 sites. Journal of Petrology 43, 1207-1239.

Gao, L.E., Zeng, L.S., Xie, K.J., 2012. Eocene high grade metamorphism and crustal anatexis in the North Himalaya Gneiss Domes, Southern Tibet. Chinese Science Bulletin 57, 639-650.

Gao, L.E., Zeng, L.S., Liu, J., Xie, K.J., 2009. Early Oligocene Na-rich peraluminous leucogranites in the Yardoi gneiss dome, southern Tibet: Formation mechanism and tectonic implications. Acta Petrologica Sinica 25, 2289-2302.

Garzanti, E., 1999. Stratigraphy and sedimentary history of the Nepal Tethys Himalaya passive margin. Journal of Asian Earth Sciences 17, 805-827.

Garzanti, E., 1993. Himalayan ironstones, "superplumes", and the breakup of Gondwana. Geology 21, 105-108.

Ghatak, A., Basu, A.R., 2013. Isotopic and trace element geochemistry of alkalic–mafic–ultramafic–carbonatitic complexes and flood basalts in NE India: Origin in a heterogeneous Kerguelen plume. Geochimica et Cosmochimica Acta 115, 46-72.

Ghatak, A., Basu, A.R., 2011. Vestiges of the Kerguelen plume in the Sylhet Traps, northeastern India. Earth and Planetary Science Letters 308, 52-64.

Ghiorso, M.S., Sack, R.O., 1995. Chemical mass transfer in magmatic processes IV. A revised and internally consistent thermodynamic model for the interpolation and extrapolation of liquid-solid equilibria in magmatic systems at elevated temperatures and pressures. Contributions to Mineralogy and Petrology 119, 197-212.

Gibson, S.A., Thompson, R.N., Dickin, A.P., Leonardos, O.H., 1995. High-Ti and Low-Ti mafic potassic magmas: Key to plum-lithosphere interactions and continental flood-basalt genesis. Earth and Planet Science Letters 136, 149-165.

Gibson, S.A., Thompson, R.N., Dickin, A.P., Leonardos, O.H., 1996. Erratum to High-Ti and Low-Ti mafic potassic magmas: Key to plum-lithosphere interactions and continental flood-basalt genesis. Earth and Planet Science Letters 141, 325-341.

Hao, Y.L., Zhang, Z.C., Wang, F.S., Mahoney, J.J., 2004. Petrogenesis of high-Ti and low-Ti basalts from the Emeishan Large Igneous Province. Geological Review 50, 587-592.

Hellman, P.L. Green, T.H., 1979. The role of sphene as an accessory phase in the high-pressure partial melting of hydrous mafic compositions. Earth and Planetary Science Letter 42, 191-201.

Hergt, J.M., Peate, D.W., Hawkesworth, C.J., 1991.The petrogenesis of Mesozoic Gondwana low-Ti flood basalts. Earth and Planetary Science Letters 105, 134-148.

Herzberg C., Asimow P.D., 2015. PRIMELT3 MEGA.XLSM software for primary magma calculation: Peridotite primary magma MgO contents from the liquidus to the solidus. Geochemistry, Geophysics, Geosystems 16, 563-578, doi: 10.1002/2014GC005631.

Hess, P.C., 1993. Phase equilibria constraints on the origin of ocean floor basalts. Mantle flow and melt generation at mid-ocean ridges. In: Morgan, J.P., Blackman, D.K., Sinton, J.M., (Eds.), Mantle flow and melt generation at Mid-Ocean Ridges, 67-102.

Hofmann, A.W., Jochum, K.P., Seufert, M., White, W.M., 1986. Nb and Pb in oceanic basalts: new constraints on mantle evolution. Earth and Planetary Science Letters 79, 33-45.

Hofmann, A.W., 1997. Mantle plume from ancient oceanic crust. Earth and Planetary Science Letters 57, 421-436.

Hou, T., Zhang, Z.C., Kusky, T., Du, Y.S., Liu, J.L., Zhao, Z.D., 2011. A reappraisal of the high-Ti and low-Ti classification of basalts and petrogenetic linkage between basalts and mafic–ultramafic intrusions in the Emeishan Large Igneous Province, SW China. Ore Geology Reviews 41, 133-143.

Hou, Z., Zheng, Y., Zeng, L., Gao, L., Huang, K., Li, W., Li, Q., Fu, Q., Liang, W., Sun, Q., 2012. Eocene–Oligocene granitoids in southern Tibet: Constraints on crustal anatexis and tectonic evolution of the Himalayan orogen. Earth and Planetary Science Letters 349-350, 38-52.

Horan, M.F., Walker, R.J., Fedorenko, V.A., Czamanske, G.K., 1995. Osmium and neodymium isotopic constraints on the temporal and spatial evolution of Siberian flood basalt sources. Geochimica et Cosmochimica Acta 59, 5159-5168.

Jackson, M.G., Hart, S.R., 2006. Strontium isotopes in melt inclusions from Samoan basalts: Implications for heterogeneity in the Samoan plume. Earth and Planetary Science Letters 245, 260-277.

Jackson, M.G., Dasgupta, R., 2008. Compositions of HIMU, EM1, and EM2 from global trends between radiogenic isotopes and major elements in ocean island basalts. Earth and Planetary Science Letters 276, 175-186.

Jackson, M.G., Weis, D., Huang, S.C., 2012. Major element variations in Hawaiian shield lavas: Source features and perspectives from global ocean island basalt (OIB) systematics. Geochemistry, Geophysics, Geosystems 13, Q09009, doi:10.1029/2012GC004268.

Juster, T.C., Grove, T.L., Perfit, M.R., 1989. Experimental constraints on the generation of FeTi basalts, andesites, and rhyodacites at the Galapagos Spreading Center, 85 W and 95 W. Journal of Geophysical Research: Solid Earth 94, 9251-9274.

Ji, W.Q., Wu, F.Y., Chung, S.L., Wang, X.C., Liu, C.Z., Li, Q.L., Liu, Z.C., Liu, X.C., Wang, J.G., 2016. Eocene Neo-Tethyan slab breakoff constrained by 45 Ma oceanic island basalt–type magmatism in southern Tibet. Geology 44, 283-286.

Klein, E.M., Karsten, J.L., 1995. Ocean-ridge basalts with convergent-margin geochemical affinities from the Chile Ridge. Nature 374, 52-57.

Kent, R.W., Saunders, A.D., Kempton, P.D., Ghose, N.C., 1997. Rajmahal basalts, eastern India: mantle sources and melt distribution at a volcanic rifted margin. In: Mahoney, J.J., Coffin, M.F., (Eds.), Large Igneous Provinces: Continental, Oceanic and Planetary Flood Volcanism. Geophysical Monograph, American Geophysical Union 100, 145-182.

Lai, S., Qin, J., Li, Y., Li, S., Santosh, M., 2012. Permian high Ti/Y basalts from the eastern part of

the Emeishan Large Igneous Province, southwestern China: Petrogenesis and tectonic implications. Journal of Asian Earth Sciences 47, 216-230.

Lassiter, J.C., DePaolo, D.J., 1997. Plume/lithosphere interaction in the generation of continental and oceanic flood basalts: chemical and isotopic constraints. Large igneous provinces: Continental, oceanic, and planetary flood volcanism, 335-355.

Li, G., Liu, X., Alex, P., Wei, L., Liu, X., Huang, F., Zhou, X., 2010. In-situ detrital zircon geochronology and Hf isotopic analyses from Upper Triassic Tethys sequence strata. Earth and Planetary Science Letters 297, 461-470.

Lightfoot, P.C., Hawkesworth, C.J., Hergt, J., Naldrett, A.J., Fedorenko, V.A., Doherty, W., 1993. Remobilisation of the continental lithosphere by a mantle plume: major-, trace-element, and Sr-, Nd- and Pb-isotope evidence from picritic and tholeiitic lavas of the Noril'sk District, Siberian Trap, Russia. Contributions to Mineralogy and Petrology 114, 171-188.

Liu, G., Ensele, G., 1994. Sedimentary history of the Tethyan basin in the Tibetan Himalayas. Geologische Rundschau 82, 32–61.

Liu, Y.Q., Qiang, J., Jiang, X.J., Kuang, H.W., Ji, S., Gao, L.F., Zhang, Z.G., Peng, N., Yuan, C.X., Wang, X.R., Xu, H., 2013. U-Pb zircon ages of Early Cretaceous volcanic rocks in the Tethyan Himalaya at Yangzuoyong Co Lake, Nagarze, Southern Tibet, and implications for the Jurassic/Cretaceous Boundary. Cretaceous Research 40, 90-101.

Liu, Z., Zhou, Q., Lai, Y., Qing, C.S., Li, Y.X., Wu, J.Y., Xia, X.B., 2015. Petrogenesis of the Early Cretaceous Laguila bimodal intrusive rocks from the Tethyan Himalaya: Implications for the break-up of Eastern Gondwana. Lithos 236-237, 190-202.

Ludden, J.N., Thompson, G., 1978. Bahavior of trace earth elements during submarine weathering

of tholeiitic basalts. Nature 274, 147-149.

Mahoney, J.J., Macdougall, J.D., Lugmair, G.W. 1983. Kerguelen hotspot source for Rajmahal traps and Ninetyeast Ridge? Nature 303, 385-389.

Mallmann, G., O'Neill, H., 2013. Calibration of an empirical thermometer and oxybarometer based on the partitioning of Sc, Y and V between olivine and silicate melt. Journal of Petrology 54, 933-949.

Mallmann, G., O'Neill, H., 2009. The Crystal/Melt partitioning of V during mantle melting as a function of oxygen fugacity compared with some other elements (Al, P, Ca, Sc, Ti, Cr, Fe, Ga, Y, Zr, and Nb). Journal of Petrology 50, 1765-1794.

Melluso, L., Srivastava, R.K., Petrone, C.M., Guarino, V., Sinha, A.K., 2012. Mineralogy and magmatic affinity of the Jasra intrusive complex, Shillong Plateau, India. Mineralogical Magazine 76, 1099-1117.

Neal, C.R., Mahoney, J.J., Chazey, W.J., 2002. Mantle sources and the highly variable role of continental lithosphere in basalt petrogenesis of the Kerguelen Plateau and Broken Ridge LIP: results from ODP Leg 183. Journal of Petrology 43, 1177-1205.

Nielsen, R.L., Gallahan, W.E., Newberger, F., 1992. Experimentally determined mineral-melt partition coefficients for Sc, Y and REE for olivine, orthopyroxene, pigeonite, magmetite amd ilmenite. Contributions to Mineralogy and Petrology 110, 488-499.

Peate, D.W., Hawkesworth, C.J., Mantovani M.M., 1992. Chemical stratigraphy of the Parana lavas (South America): classification of magma types and their spatial distribution. Bulletion of Volcanology 55,119-139.

Peate, D.W., Hawkesworth, C.J., 1996. Lithospheric to asthenospheric transition in low-Ti flood

basalts from southern Parana, Brazil. Chemical Geology 127, 1-24.

Petrini, R., Civetta, L., Piccirillo, E.M., Bellieni, G., Comin-Chiaramonti, P., Marques, L.S., Melfi, A.J., 1987. Mantle heterogeneity and crustal contamination in the genesis of low-Ti continental flood basalts from the Paraná plateau (Brazil): Sr–Nd isotope and geochemical evidence. Journal of Petrology 28, 701-726.

Prytulak, J., Elliott, T., 2007. TiO_2 enrichment in ocean island basalts. Earth and Planetary Science Letters 263, 388-403.

Qi, X.X., Zeng, L.S., Meng, X.J., Xu, Z.Q., Li, T.F., 2008. Zircon SHRIMP U-Pb dating for Dala granite in the Tethyan Himalaya and its geological implication. Acta Petrologica Sinica 24, 1501-1508.

Ren, Z.Y., Wu, Y.D., Zhang, L., Nichols, A.R., Hong, L.B., Zhang, Y.H., Zhang, Y., Liu, J.Q., Xu, Y.G., 2017. Primary magmas and mantle sources of Emeishan basalts constrained from major element, trace element and Pb isotope compositions of olivine-hosted melt inclusions. Geochimica et Cosmochimica Acta, In press.

Rollinson, H.R., 1993. Using geochemical data: evaluation, presentation, interpretation (New York, Wiley), 108-352.

Rudnick, R.L., Gao, S., 2003. The composition of the continental crust. In: Rudnick RL (Eds.), The Crust, 1–64.

Ryerson, F., Watson, E., 1987. Rutile saturation in magmas: implications for Ti–Nb–Ta depletion in island-arc basalts. Earth and Planetary Science Letters 86, 225–239.

Said, N., Kerrich, R., 2010. Magnesian dyke suites of the 2.7 Ga Kambalda Sequence, Western Australia: evidence for coeval melting of plume asthenosphere and metasomatised

lithospheric mantle. Precambrian Research 180, 183-203.

Shellnutt, J.G., Jahn, B.M., 2011. Origin of Late Permian Emeishan basaltic rocks from the Panxi region (SW China): Implications for the Ti-classification and spatial–compositional distribution of the Emeishan flood basalts. Journal of Volcanology and Geothermal Research 199, 85-95.

Simonetti, A., Goldstein, S.L., Schmidberger, S.S., Viladkar, S.G., 1998. Geochemical and Nd, Pb, and Sr isotope data from Deccan alkaline complexes—inferences for mantle sources and plume–lithosphere interaction. Journal of Petrology 39, 1847-1864.

Smith, R., Smith, S., 1976. Comments on the use of Ti, Zr, Y, Sr, K, P and Nb in classification of basaltic magmas. Earth and Planetary Science Letters 32, 114-120.

Smith, P.M., Asimow, P.D., 2005. Adiabat_1ph: A new public front-end to the MELTS, pMELTS, and pHMELTS models. Geochemistry, Geophysics, Geosystems 6, Q02004, doi:10.1029/2004GC000816.

Snyder, D., Carmichael, I.S.E., Wiebe, R.A., 1993. Experimental study of liquid evolution in an Fe-rich, layered mafic intrusion: constraints of the Fe-Ti oxide precipitation on the T-fO_2 and T-ρ paths of tholeiitic magmas. Contributions to Mineralogy and Petrology 113, 73-86.

Sobolev, A.V., Hofmann, A.W., Sobolev, S.V., Nikogosian, I.K., 2005. An olivine-free mantle source of Hawaiian shield basalts. Nature 434, 590-597.

Sobolev, A.V., Hofmann, A.W., Kuzmin, D.V., Yaxley, G.M., Arndt, N.T., Chung,S.L., Danyushevsky, L.V., Elliott, T., Frey, F.A., Garcia, M.O., Gurenko, A.A., Kamenetsky, V.S., Kerr, A.C., Krivolutskaya, N.A., Matvienkov, V.V., Nikogosian, I.K., Teklay, M., 2007. The amount of recycled crust in sources of mantle-derived melts. Science 316, 412-417.

Srivastava, R.K., Sinha, A.K., 2007. Nd and Sr isotope systematics and geochemistry of a plume-related Early Cretaceous alkaline-mafic-ultramafic igneous complex from Jasra, Shillong Plateau, northeastern India. Geological Society of America Special Papers 430, 815-830.

Srivastava, R.K., Heaman, L.M., Sinha, A.K., Shihua, S. 2005. Emplacement age and isotope geochemistry of Sung Valley alkaline–carbonatite complex, Shillong Plateau, northeastern India: implications for primary carbonate melt and genesis of the associated silicate rocks. Lithos 81, 33-54.

Staudigel, H., Plank, T., White, B., Schmincke, H.U., 1996. Geochemical fluxes during seafloor alteration of the basaltic upper oceanic crust: DSDP sites 417 and 418. In: Bebout, G.E., Scholl, S.W., Kirby, S.H., Platt, J.P. (Eds.), Subduction top to bottom, 19-38.

Sun, S.S., McDonough, W.F., 1989. Chemical and isotopic systematics of oceanic basalts: implications for mantle composition and processes. Geological Society, London, Special Publications 42, 313-345.

Toplis, M.J., Carroll, M.R., 1995. An experimental-study of the influence of oxygen fugacity on Fe-Ti oxide stability, phase-relations, and mineral-melt equilibria in ferro-basaltic systems. Journal of Petrology 36, 1137-1170.

Toplis, M.J., Carroll, M.R., 1996. Differentiation of ferro-basaltic magmas under conditions open and closed to oxygen; implications for the Skaergaard intrusion and other natural systems. Journal of Petrology 37, 837-858.

Toplis, M.J., Corgne, A., 2002. An experimental study of element partitioning between magnetite, clinopyroxene and iron-bearing silicate liquids with particular emphasis on vanadium.

Contributions to Mineralogy and Petrology 144, 22-37.

Vannay, J.C., Spring, L., 1993. Geochemistry of the continental basalts within the Tethyan Himalaya of Lahul-Spiti and SE Zanskar, northwest India. Geological Society Special Publication (London) 74, 237-249.

Walker, J.A., Carr, M.J., Feigenson, M.D., Kalamarides, R.I., 1990. The Petrogenetic Significance of Interstratified High-and Low-Ti Basalts in Central Nicaragua. Journal of Petrology 31, 1141-1164.

Walker, R.J., Morgan, J.W., Horan, M.F., 1995. ^{187}Os enrichment in some mantle plume sources: evidence for core-mantle interaction? Science 269, 819-822.

Walker, R.J., Storey, M., Kerr, A.C., Tarney, J., Arndt, N.T., 1999. Implications of ^{187}Os isotopic heterogeneities in mantle plum: evidence from Gorgona island and Curacao. Geochimica et Cosmochimica Acta 63, 713-728.

Walker, R.J., Reichard, H.M., Ishiwatari, A., Pimentel, M., 2002. The osmium isotopic composition of convecting upper mantle deduced from ophiolite chromites. Geochimica et Cosmochimica Acta 66, 329-345.

Wang, C. Y., Zhou, M. F., Qi, L., 2007. Permian flood basalts and mafic intrusions in the Jinping (SW China)–Song Da (northern Vietnam) district: mantle sources, crustal contamination and sulfide segregation. Chemical Geology 243, 317-343.

Wang, Y.Y., Gao, L.E., Chen, F.K., Hou, K.J., Wang, Q., Zhao, L.H., Gao, J.H., 2016. Multiple phases of cretaceous mafic magmatism in the Gyangze-Kangma area, Tethyan Himalaya, southern Tibet. Acta Petrologica Sinica 32, 3572-3596.

Webb, A.A.G., Yin, A., Dubey, C.S., 2013. U-Pb zircon geochronology of major lithologic units in

the eastern Himalaya: Implications for the origin and assembly of Himalayan rocks. Geological Society of America Bulletin 125, 499-522.

White, W.M., 2015. Isotopes, DUPAL, LLSVPs, and Anekantavada. Chemical Geology 419, 10-28.

Williams, H., Turner, S., Kelley, S., Harris, N., 2001. Age and composition of dikes in Southern Tibet: New constraints on the timing of east-west extension and its relationship to postcollisional volcanism. Geology 29, 339-342.

Xia, Y., Zhu, D.C., Wang, Q., Zhao, Z.D., Liu, D., Wang, L.Q., Mo, X.X., 2014. Picritic porphyrites and associated basalts from the remnant Comei Large Igneous Province in SE Tibet: records of mantle-plume activity. Terra Nova 26, 487-494.

Xiao, L., Xu, Y.G., Mei, H.J., Zheng, Y.F., He, B., Pirajno, F., 2004. Distinct mantle sources of low-Ti and high-Ti basalts from the western Emeishan large igneous province, SW China: implications for plume–lithosphere interaction. Earth and Planetary Science Letters 228, 525-546.

Xie, K.J., Zeng, L.S., Liu, J., Gao, L.E., 2010. Late-Eocene Dala adakitic granite, southern Tibet and geological implications. Acta Petrologica Sinica 26, 1016-1026.

Xu, Y.G., Chung, S.L., Jahn, B., Wu, G., 2001. Petrologic and geochemical constraints on the petrogenesis of Permian–Triassic Emeishan flood basalts in southwestern China. Lithos 58, 145-168.

Xu, Y., Mei, H., Xu, J., Huang, X., Wang, Y., Chung, S.L., 2003. Origin of two differentiation trends in the Emeishan flood basalts. Chinese Science Bulletin 48, 390-394.

Xu, Y.G., He, B., Chung, S.L., Menzies, M.A., Frey, F.A., 2004. Geologic, geochemical, and

geophysical consequences of plume involvement in the Emeishan flood-basalt province. Geology 32, 917-920.

Zeng, L.S., Gao, L-E., Guo, C.L., Hou, K.J., Wang, Q., 2017. Early Cretaceous forearc extension of the Gangdese continental arc, southern Tibet. Acta Petrologica Sinica, 33, 2377-2394.

Zeng, L.S., Wang, Y.H., Gao, L.E., Wang, Y.Y., 2016. Elusive Cenozoic metamorphism in mafic dike swarms within the Tethyan Himalaya, southern Tibet. Acta Geologica Sinica 90, 86-97.

Zeng, L.S., Gao, L.E., Shang, Z., Gao, J.H., Wang, Y.Y., 2015a. The metamorphism in mafic dike swarms from Eocene to Oligocene within the Tethyan Himalaya, southern Tibet. Acta Geologica Sinica 89, 309-312.

Zeng, L.S., Gao, L.E., Tang, S.H., Hou K.J., Guo, C.L., Hu, G.Y., 2015b. Eocene magmatism in the Tethyan Himalaya, southern Tibet. Geological Society, London, Special Publications, 412, 287-316.

Zeng, L.S., Gao, L-E., He, K.J., Tang, S.H., Guo, C.L., 2012a. Multiple Mafic Magmatic Events along the Tethyan Himalaya: Tracing the Life-time of the Neo-Tethyan Ocean. Acta Geoscientica Sinica 33, 72-73.

Zeng, L.S., Gao, L.E., Hou, K.J., Tang S.H., 2012b. Late Permian mafic magmatism along the Tethyan Himalaya Belt, southern Tibet and tectonic implications. Acta Petrologica Sinica 28, 1731-1740.

Zeng, L., Gao, L., Xie, K., Liu-Zeng, J., 2011a. Mid-Eocene high Sr/Y granites in the Northern Himalayan Gneiss Domes: Melting thickened lower continental crust. Earth and Planetary Science Letters 303, 251-266.

Zeng, L.S., Gao, L.E., Xie, K.J., 2011b. Concurrence of Mid-Miocene high Sr/Y granite and

leucogranite in the Yardoi gneiss dome, Tethyan Himalaya, Southern Tibet. Mineralogical Magazine 75, 2245.

Zeng, L.S., Liu, J., Gao, L.E., Xie, K.J., Wen, L., 2009. Early Oligocene anatexis in the Yardoi gneiss dome, southern Tibet and geological implications. Chinese Science Bulletin 54, 104-112

Zhu, D.C., Chung, S.L., Mo, X.X., Zhao, Z.D., Niu, Y.L., Song, B., Yang, Y.H., 2009. The 132 Ma Comei-Bunbury large igneous province: Remnants identified in present-day southeastern Tibet and southwestern Australia. Geology 37, 583-586.

Zhu, D.C., Mo. X.X., Pan, G.T., Zhao, Z.D., Dong, G.C., Shi, Y.R., Liao, Z.L., Wang, L.Q., Zhou. C.Y., 2008. Petrogenesis of the earliest Early Cretaceous mafic rocks from the Cona area of the eastern Tethyan Himalaya in south Tibet: Interaction between the incubating Kerguelen plume and the eastern Greater India lithosphere? Lithos 100, 147-173.

Zhu, D.C., Pan, G.T., Mo, X.X., Liao, Z.L., Jiang, X.S., Wang, L.Q., Zhao, Z.D., 2007. Petrogenesis of volcanic rocks in the Sangxiu Formation, central segment of Tethyan Himalaya: A probable example of plume–lithosphere interaction. Journal of Asian Earth Sciences 29, 320-335.

Figure and table captions

Fig. 1 (A) Physiographic map of the Indian Ocean and surrounding continents, showing spatial-temporal locations of the Comei LIP and other products created by the Kerguelen plume, after Zhu et al., 2008; (B) Sketch tectonic map of the east-central Tethyan Himalaya and eastern India showing the present locations of the Comei LIP, the Rajmahal and Sylhet Traps of eastern India (Zhu et al., 2008; Zeng et al., 2009); (C) Simplified geologic map showing spatial extent and distributions of ~132 Ma igneous rocks of the remnant Comei LIP (Zhu et al., 2009). Square frame with arrows indicates the locations of samples: Cona samples are from Zhu et al., 2008, Xia et al., 2014, and Liu et al., 2015. Rimowa samples are from Zhu et al., 2007. Gyangze samples are from Wang et al., 2016. Dala samples are from this paper.

Fig. 2 Simplified geologic map of the Dala study area, at the southeast extreme of the Yardoi gneiss dome in the eastern Tethyan Himalaya, southern Tibet.

Fig. 3 Photomicrographs and BSE image showing different mineral assemblages and textures of Dala diabase. Panels (a) and (b) are from Sample T0766-2 (group 1) and T0766-8 (group 2), the high-Mg/low-Ti examples. Panels (c), (d) and (e) are from Sample T0766-14, T0766-15 (group 3), and T0766-17 (group 4), respectively, the low-Mg/high-Ti examples. Panel (f) shows ilmenite grain surrounded by titanite from Sample T0766-13 (group 3). Hbl-hornblende; Chl-chlorite replacing pyroxene; Bt-biotite; Pl-plagioclase; Ilm-ilmenite; Ttn-titanite.

Fig. 4 U-Pb concordia and age distribution diagrams for concordant zircons from

samples T0766-1 and T0766-8; xenocrystic grains with ages near 190 Ma are not included.

Fig.5 Variation diagrams of (a) TiO_2 and (b) Ti/Y against MgO for the Dala diabases.

Fig.6 Variation diagrams of selected major oxides (wt%) and ratios versus MgO (wt%) for Dala diabases. The three lines are liquid lines of descent modeled with the software *alphaMELTS* at 3000 bars, QFM+1; 5000 bars, QFM+1; and 3000 bars, QFM-1, respectively, from a primitive magma composition calculated by *PRIMELT3* and assuming 0.1 wt% initial H_2O content.

Fig. 7 Variation diagrams of selected trace elements (ppm) versus major elements MgO, TiO_2 or P_2O_5 (wt%) for Dala diabases. Symbols as in legend of Fig.5.

Fig. 8 (a) Chondrite-normalized rare earth element patterns and (b) primitive-mantle normalized multi-trace element patterns for Dala diabase.

Data for chondrite, primitive mantle and OIB normalization values are from Sun and McDonough (1989).

Fig.9 (a) $(Th/Nb)_{PM}$ vs. $(La/Nb)_{PM}$ and (b) Nb/U-Ce/Pb diagrams to show the crust-like signature from the trace element characteristics for Dala diabase (after Neal et al., 2002; Klein and Karsten, 1995. MC-middle crust and LC-lower crust are from Rudnick and Gao, 2003.)

Fig. 10 $^{87}Sr/^{86}Sr(t)$ vs. $\varepsilon_{Nd}(t)$ (a-b) and Nb/La vs. $\varepsilon_{Nd}(t)$ (c) diagrams for Dala diabases. Altered samples are not shown in panel c. Magmatic products from Comei LIP are from Zhu et al., 2007&2008; Xia et al., 2014; Liu et al., 2015; Wang et al., 2016. The shaded areas are basalts related with the Kerguelen plume. Data sources:

Ninety-Eastern Ridge, Kerguelen Plateau, Heard Island and Broken Ridge (Frey et al., 2000 and related references), Bunbury Gosselin and Bunbury Casuarina (Frey et al., 1996), Rajmahal Traps (Kent et al., 1997). Early Cretaceous subcontinental lithospheric mantle in NE India data inferred by the contemporaneous mantle-derived alkaline-carbonatite complexes from Srivastava et al., 2005; Melluso et al., 2012.

Fig.11 Hf isotope compositions in zircon grains from the Dala diabase.

Fig.12 Covariation diagrams of TiO_2 (wt%) versus $\varepsilon_{Nd}(t)$ (**a**), Nb/La (**b**) and MgO (wt%) (**c**) for mafic rocks in Comei LIP. Data sources are same as Fig.10, and altered samples are removed. The typical liquid line of descent (LLD) of a primary OIB composition is from Prytulak and Elliott (2007).

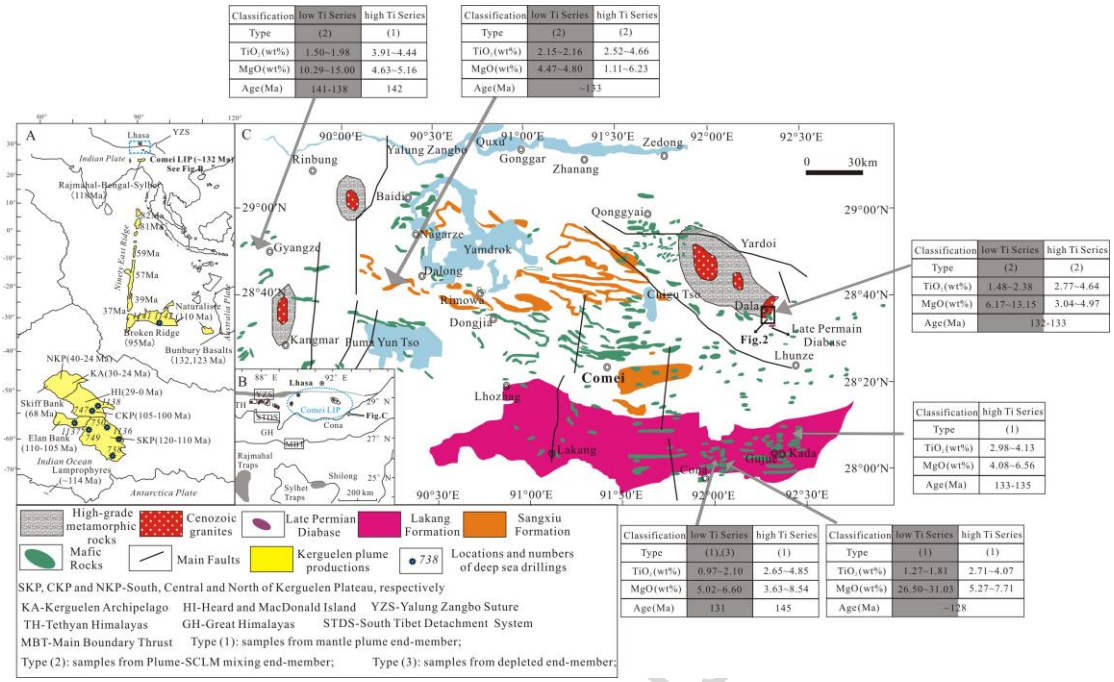

Figure 1

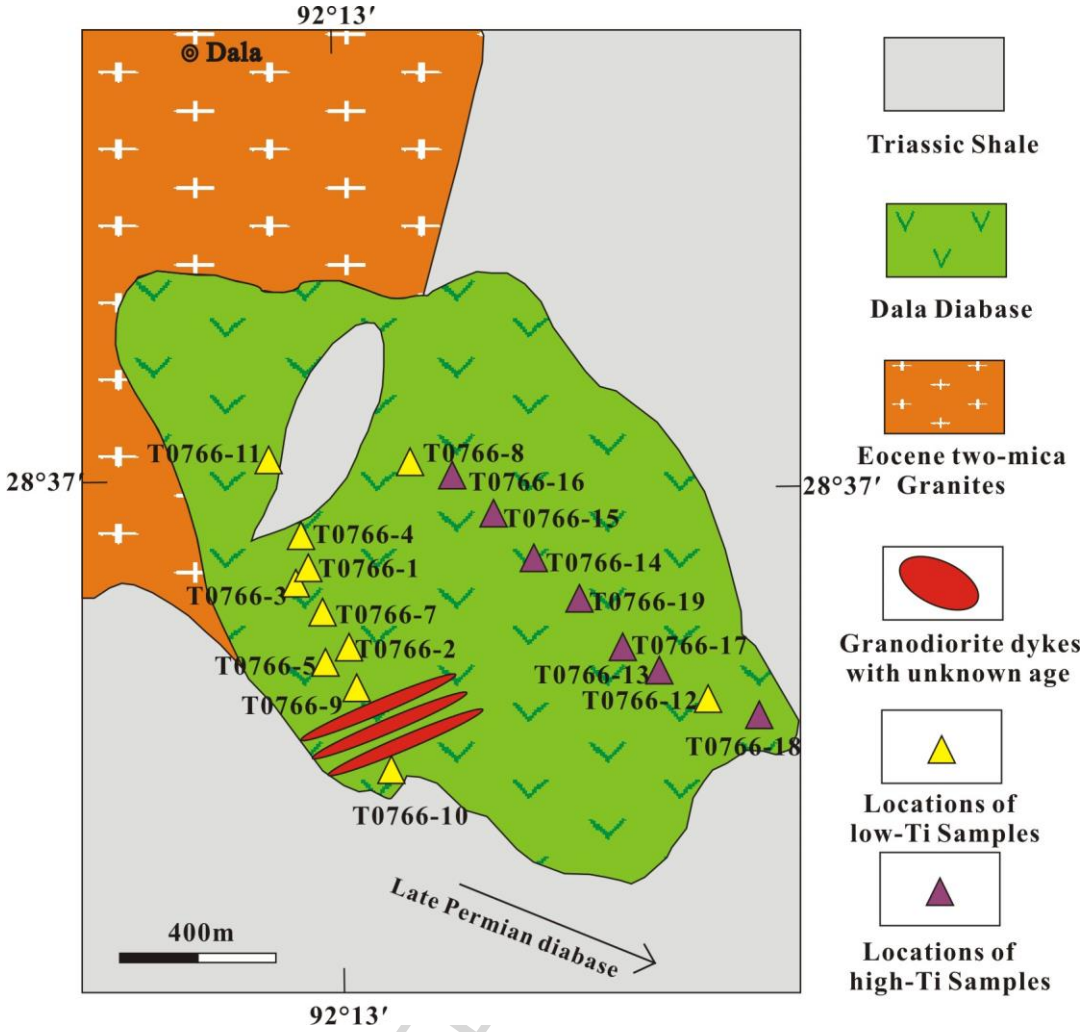

Figure 2

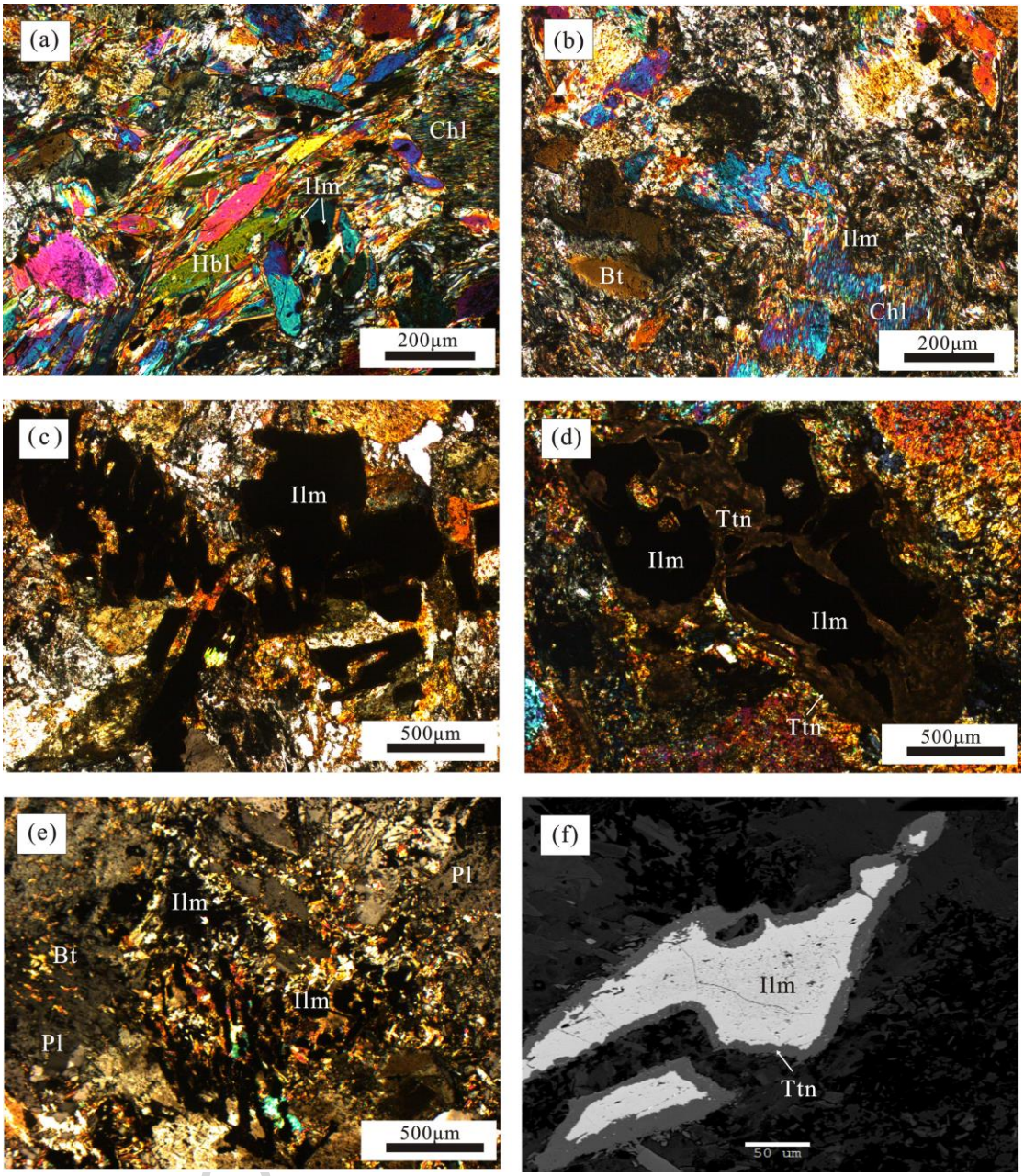

Figure 3

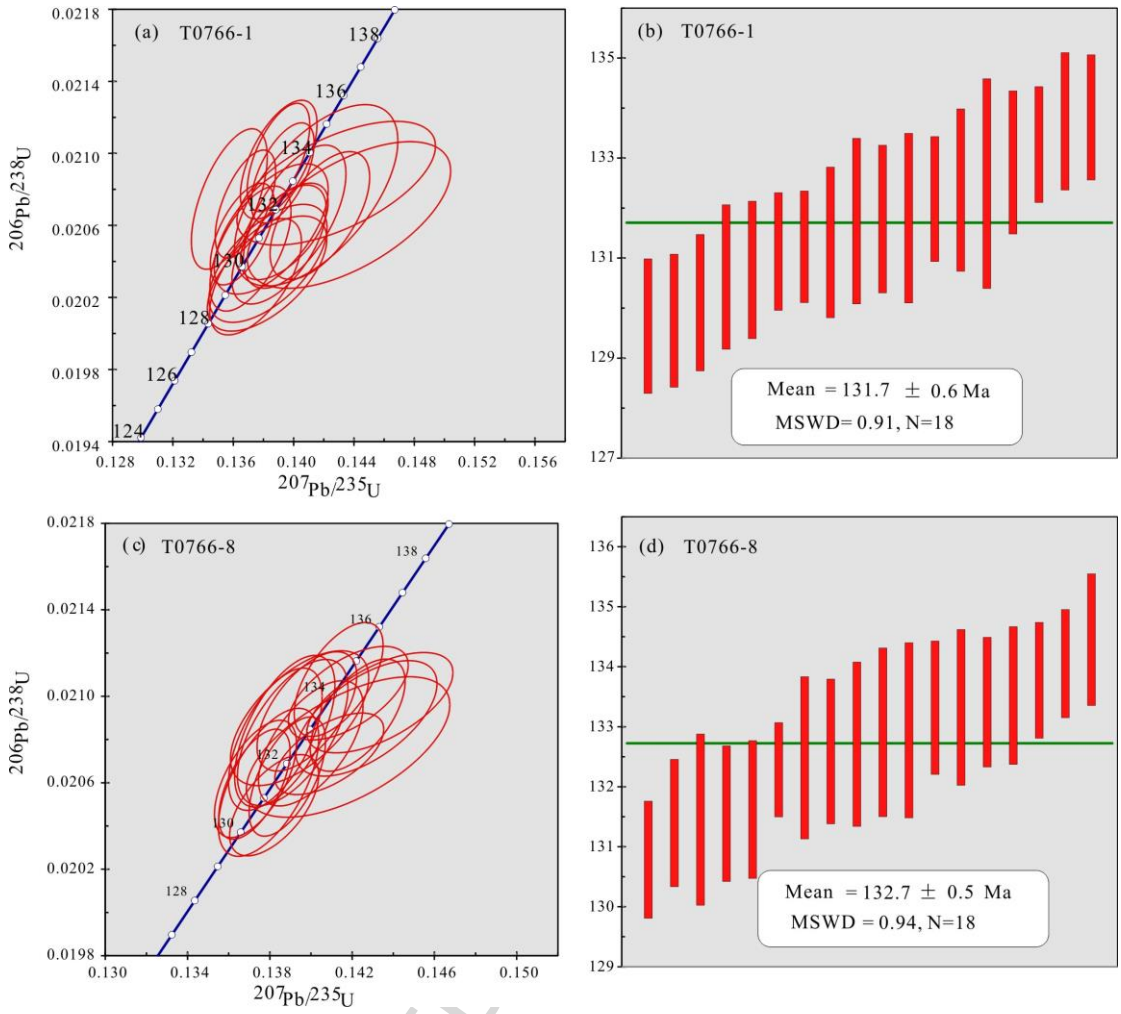

Figure 4

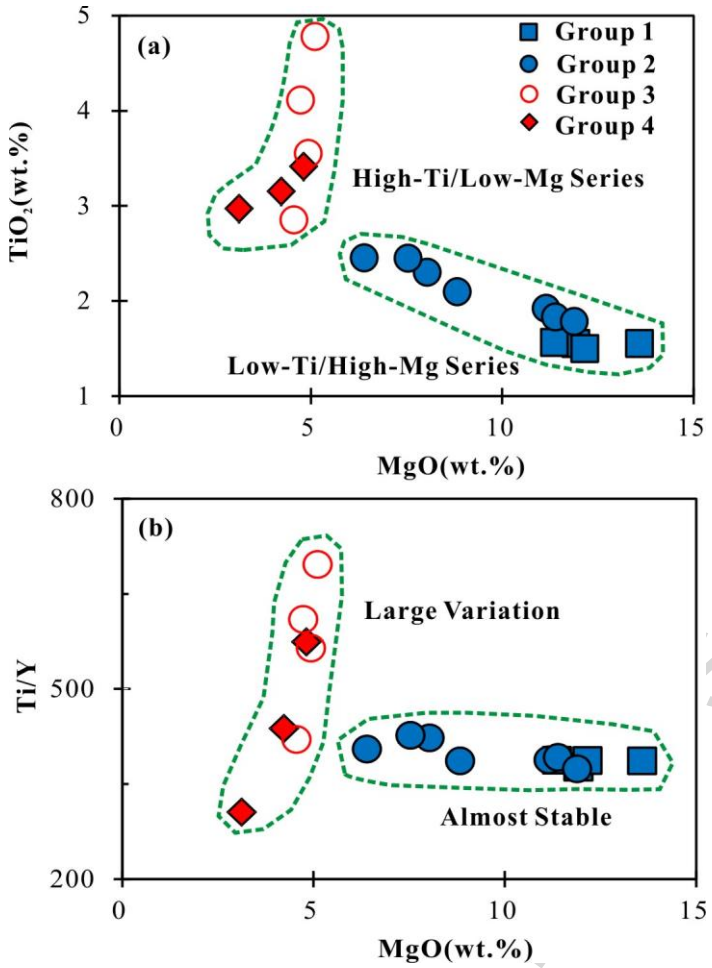

Figure 5

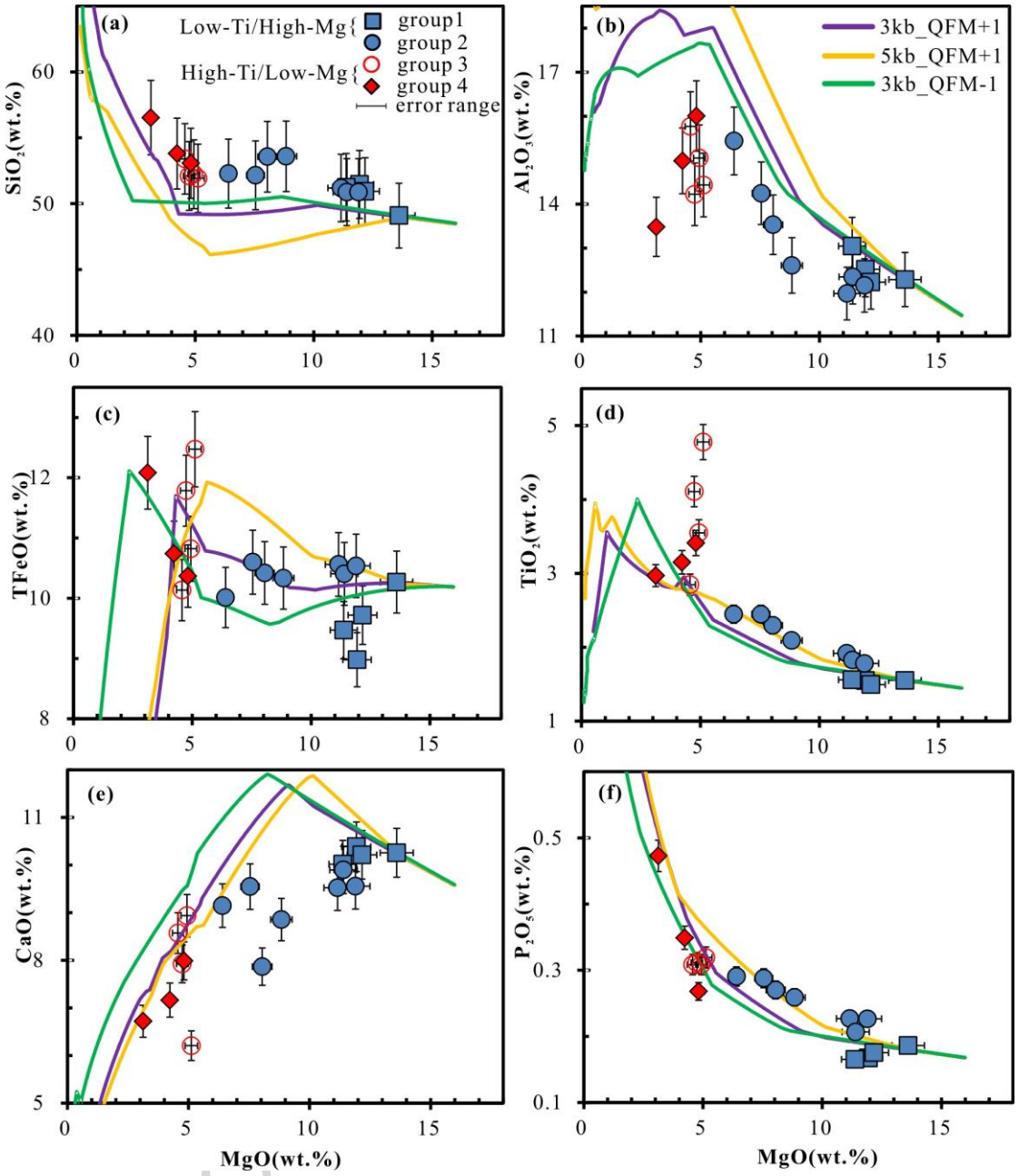

Figure 6

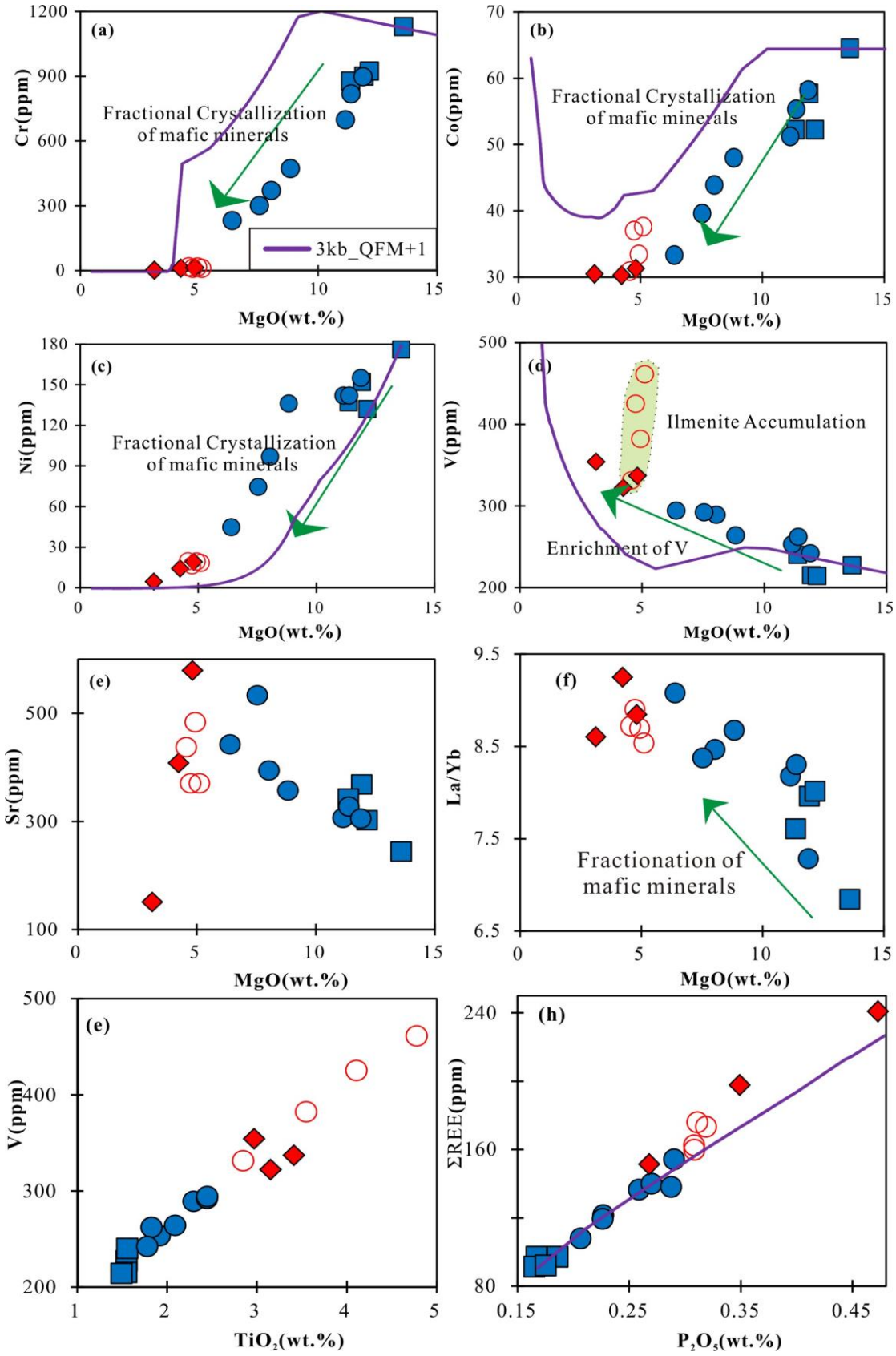

Figure 7

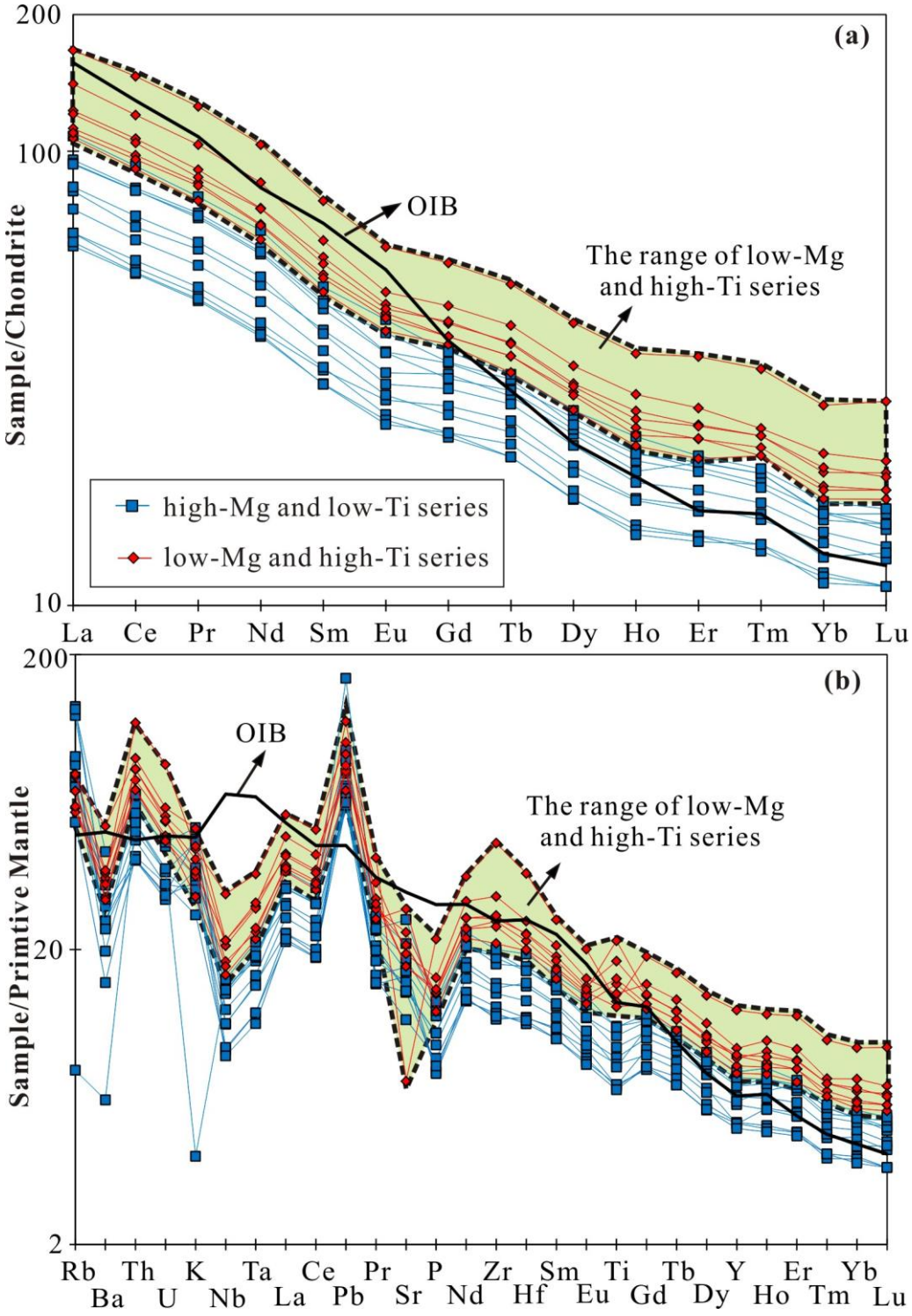

Figure 8

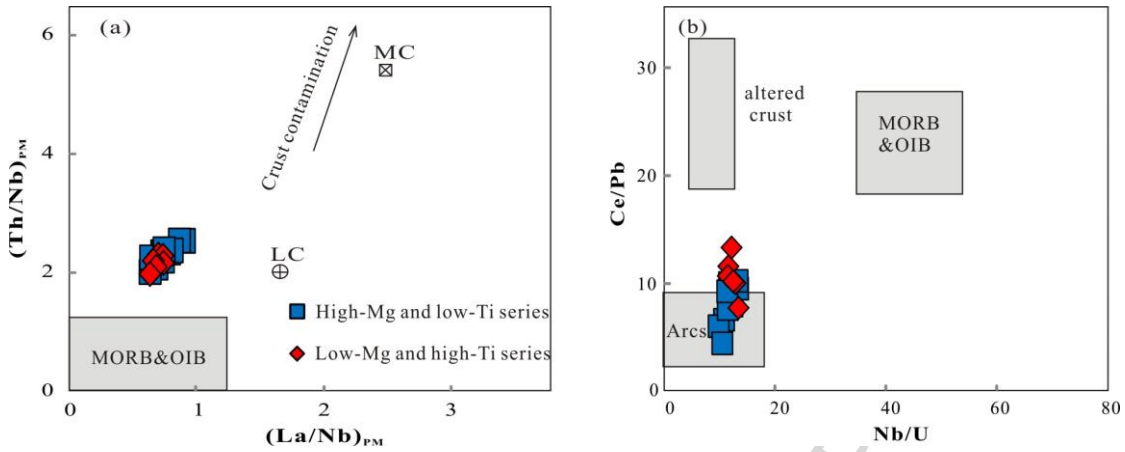

Figure 9

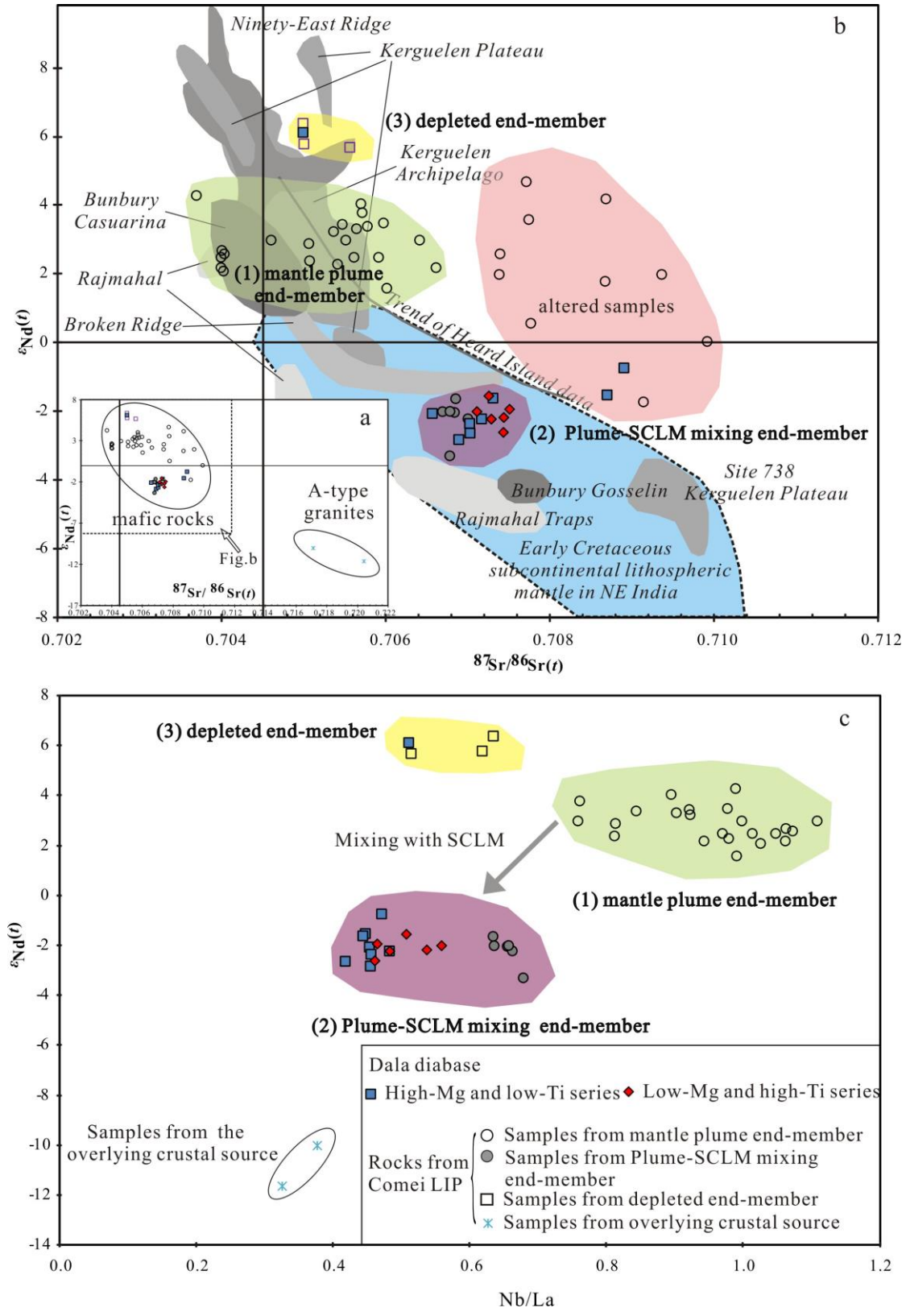

Figure 10

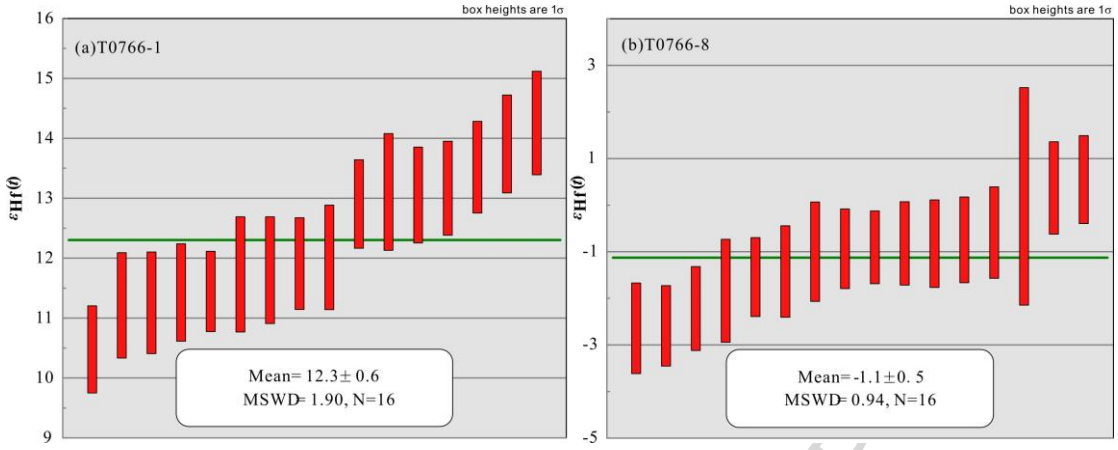

Figure 11

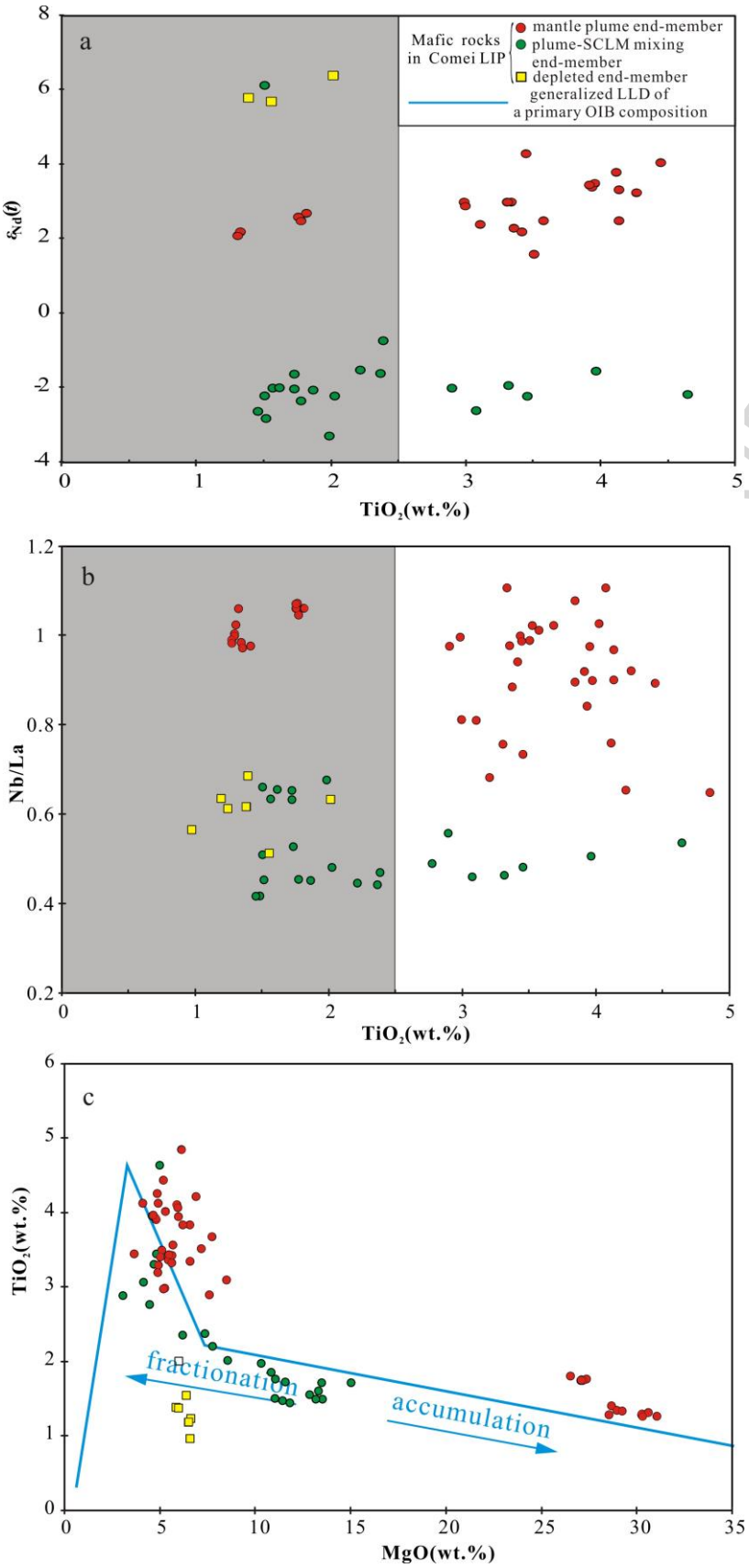

Figure 12

Highlights

1. The Dala diabase intrusion, belongs to the ~132 Ma Comei LIP and represents interaction between Kerguelen plume and subcontinental lithosphere.

2. The low-Ti and high-Ti series of Dala diabase represent progressive fractional crystallization from one primary source except for samples with ilmenite accumulation.

3. Ti contents of evolved magmas in LIP cannot be quantitatively related to source processes without correct for fractionation.